NOAA Technical Report NESDIS 68

AMSU-A ENGINEERING MODEL CALIBRATION

Washington, D.C.
June 1993

U.S. DEPARTMENT OF COMMERCE
National Oceanic and Atmospheric Administration
National Environmental Satellite, Data, and Information Service

NOAA Technical Report NESDIS 68

AMSU-A ENGINEERING MODEL CALIBRATION

Tsan Mo, Michael P. Weinreb and Norman C. Grody
Office of Research and Applications
Satellite Research Laboratory

and

David Q. Wark
Office of Research and Applications

Washington, D.C.
June 1993

U.S. DEPARTMENT OF COMMERCE
Ronald H. Brown, Secretary

National Oceanic and Atmospheric Administration
Diana H. Josephson, Acting Under Secretary

National Environmental Satellite, Data, and Information Service
Gregory W. Withee, Acting Assistant Administrator

TABLE OF CONTENTS

Table Captions

Figure Captions

ABSTRACT

Thermal-vacuum calibration data generated from the Advanced Microwave Sounding Unit-A (AMSU-A) Engineering Model (EM) were analyzed for assessing the instrument's performance and the results were compared to the required specifications. A new calibration algorithm, which represents a scene target-view radiance in terms of radiometric counts was developed and tested with the calibration data. Nonlinear contribution due to an imperfect square-law detector was incorporated into the calibration algorithm via a nonlinearity parameter, μ, of which values were determined by least-squares fit of a set of data taken at a fixed instrument temperature. The analysis covers the calibration accuracy, nonlinearity, and radiometric temperature sensitivity (NEΔT). We found that all specifications are met by the results derived from the thermal-vacuum chamber test data, except the NEΔT values (0.34K and 0.52K) at channels 9 and 15 (57.29 and 89.0 GHz), which exceed the required specification of 0.25K and 0.5K, respectively, for the two channels. The manufacturer found that the large NEΔT value at channel 9 was due to un-optimized mixer and its requirement was waived. The NEΔT value at channel 15 exceeds the limit by a small margin and probably meets the requirement within measurement uncertainty. For each channel, a warm target fixed bias correction factor, which plays an important role in this analysis, is incorporated into the calibration algorithm. These fixed bias correction factors (supplied by Aerojet) also depend upon the instrument temperatures. This analysis of the AMSU-A data provides us with a better understanding of the instrument's functioning. Experience and information gained from this work provide useful insights into the development of computer software for processing the NOAA-K,L,M data collected from space in the future.

1. INTRODUCTION

The AMSU-A is a new generation of total-power microwave radiometer containing 15 channels to retrieve vertical atmospheric temperature and water vapor profiles up to the upper stratosphere. These instruments will be flown on the NOAA-K, -L, and -M series of polar-orbiting satellites. The AMSU-A antenna will have a field-of-view 3.3 degrees at the half-power points and will provide a crosstrack scan of $\pm$48.33 degrees from the nadir direction with 30 Earth-fields-of-view per scan line. Beam positions 1 and 30 are the extreme scan positions of the Earth views, while beam position 15 looks approximately along the nadir direction. Onboard black-body and cold space calibrations will be performed for each scan line (8 seconds per scan).

Besides an EM, three AMSU-A flight models (i.e., Protoflight Model, Flight Model 1 and Flight Model 2) are being built by GenCorp/Aerojet Electronic Systems Division (AESD). Each of the AMSU-A Models will be tested and calibrated in a thermal-vacuum chamber by the

instrument builder before being launched on a NOAA satellite. The NOAA/NESDIS Office of Research and Applications (ORA) is responsible for analyzing these pre-launch calibration data from thermal-vacuum chamber tests and assessing the instrument's performance for each of the instrument models.

The thermal-vacuum chamber calibration data of the AMSU-A EM were obtained by Aerojet. In this report, we present an analysis of these calibration data. Topics covered in this analysis include calibration accuracy, nonlinearity, and radiometric temperature sensitivity (NEΔT or noise-equivalent temperature uncertainty). Section 1 gives an introduction and section 2 presents a brief description of the thermal-vacuum chamber test data. The calibration algorithm is described in section 3 and results are presented in section 4. Discussion and conclusion are given in section 5.

2. DESCRIPTION OF DATA

The central frequencies of the AMSU-A channels are listed in Table 1, which also gives the number of pass band and the channel bandwidth. The instrument specifications for temperature sensitivity and calibration accuracy are also listed in the last two columns. The AMSU-A system consists of two physically separate modules. One of the modules, AMSU-A2, provides the 23.8 and 31.4 GHz channels (channels 1 and 2, respectively) and the other module, AMSU-A1, furnishes 13 channels (channels 3 through 15) using two antenna systems, A1-1 and A1-2. The channels covered by each antenna system are listed below:

- AMSU-A2: Channels 1 and 2
- AMSU-A1-2: Channels 3, 4, 5 and 8
- AMSU-A1-1: Channels 6, 7, and 9-15

The AMSU-A EM has been tested in a thermal-vacuum chamber by Aerojet. The test data were acquired in two different modes, In-Orbit Mode and Calibration Mode, respectively. In the In-Orbit Mode (also called Full Scan Mode), AMSU-A scans through 30 different scene-view (or beam) positions, the cold calibration target, and the internal warm calibration blackbody target once every 8 seconds. It takes one look (or sample) at each scene-view position and two looks at the cold and warm calibration targets, respectively. Since the scene calibration target was located at beam position 6, only one scene target view (beam position 6) can be used for calibration. Each antenna system looks at its individual cold, warm, and scene targets, temperatures of which are measured by Platinum Resistance Thermometers (PRTs). The numbers of PRTs used to measure the physical temperatures of the scene, cold, and warm

calibration targets in each antenna system are given below:

	Scene Target	Cold Target	Warm Target
● AMSU-A1-1	7	7	5
● AMSU-A1-2	7	7	5
● AMSU-A2	11	11	7

More PRTs are used in the AMSU-A2 case because the targets are larger than those used in the first two cases.

In the Calibration Mode (also called 10-10-10 Mode), the AMSU-A moves directly to the scene target position (i.e., beam position 6) and takes 10 samples there, then goes to the cold calibration target for 10 samples. Finally, it moves to the internal warm calibration target and acquires another 10 samples. All of the three groups of samples are collected within the same scan period of 8 seconds. The advantage of the 10-10-10 mode is that it yields the same number of data samples in a shorter time than the Full-Scan mode.

The AMSU-A2 (channels 1 and 2) calibration data were taken with the In-Orbit Mode, whereas the data for channels 3-15 were acquired with the 10-10-10 Mode.

We extracted the following calibration parameters for each scan from the "raw" data tapes provided by Aerojet,

- Scene Count(s) at beam position 6 (one sample for each of the A2 channels and ten samples for each of the A1 channels)
- PRT Scene Target Temperature in degree Kelvin (average temperature over 11 PRTs for A2 and 7 PRTs for A1)
- Cold Target Counts (two samples for each of the A2 channels and ten samples for each of the A1 channels)
- PRT Cold Target Temperature in degree Kelvin (averaged over 11 PRTs for A2 and 7 PRTs for A1)
- Warm Target Counts (two samples for each of the A2 channels and ten samples for each of the A1 channels)
- Warm Load PRT Counts (one sample for each PRT)

The Warm Load PRT counts are converted to resistance and then to warm calibration target PRT temperatures, which are also corrected by the "In-Flight Warm-load Correction Factors" supplied by Aerojet for each channel.

Greater procedural details for processing these data can be found in [1]. Table 2 gives a set of 30 scan samples of the calibration data obtained under the In-Orbit Mode for channels 1 and 2 at the scene-target temperature, T_s = 84K. The counts in columns 6-8 are for channel 1, and those in columns 9-11 are for channel 2. The time for each scan is given in the second column, which shows an 8-second time interval between two scans. For each scene-target temperature, 120 scans were taken under this In-Orbit Mode. Each of the warm- and cold-target counts listed in Table 2 is the average of two looks (samples), while the scene-target count is from a single look at the scene target position 6.

Table 3 lists the sample data of a single scan acquired with the 10-10-10 Calibration Mode. The radiometric counts from the ten looks at the scene, warm, and cold targets, respectively, are listed in separate rows for each channel under the headings of A1-2 and A1-1, respectively. The PRT temperatures corresponding to the scene, warm, and cold targets are also given in the headings. Further discussion of these data will be given sections 3 and 5.

The warm-target temperature is obtained from the warm load PRT counts, C_{prt}, in two steps. First, the PRT count, C_{prt}, was converted to resistance by a count-to-resistance lookup table supplied by Aerojet. The warm-target temperature, t, is then computed from the PRT resistance, R_t, using the Callendar-Van Dusen equation [2]:

$$\frac{R_t}{R_o} = 1 + \alpha\left[t - \delta\left(\frac{t}{100} - 1\right)\left(\frac{t}{100}\right) - \beta\left(\frac{t}{100} - 1\right)\left(\frac{t}{100}\right)^3\right] \qquad (1)$$

where:
R_t = resistance (in ohms) at temperature, t (°C) of the warm target
R_o = resistance at t = 0°C (supplied by the manufacturer, Wahl Instrument)
β = 0 for t > 0°C, and 0.11 for t < 0°C
α and δ are constants provided by the manufacturer, Wahl Instrument.

Equation (1) is quartic for t < 0°C, but becomes quadratic for t > 0°C. For each case, t can be solved in terms of R_t. However, the β term was omitted in the computer software package

supplied by Aerojet. According to reference [3], the error due to this omission is very small. For a given R_t, the t value is obtained from Equation (1) using a computer subroutine extracted from the Aerojet-supplied software package. The warm-target temperature in degree Kelvin for each PRT reading is obtained from $T_w = 273.15 + t$.

Radiance is linearly proportional to brightness temperature above 50K in the AMSU-A spectral region (Rayleigh-Jeans approximation). In this study, we use radiance for representing all measurements. This choice will eliminate any frequency-dependent error and it does not require any modification of the representation at low brightness temperatures near the cold space region 2.73K. We convert all brightness temperatures into radiances using the Planck function, $B(\nu,T)$, which is given by

$$B(\nu,T) = \frac{(2hc^2)\nu^3}{\exp\left(\frac{ch\nu}{kT}\right) - 1} \qquad (2)$$

According to the most recent recommendation by the Committee on Data (CODATA) for Science and Technology of the International Council of Scientific Unions in 1986 [4], values of the fundamental physical constants in Equation (2) are: c = speed of light = 2.997925×10^{10} cm/sec, h = Planck's constant= 6.626076×10^{-34} Joules-sec, and k = Boltzmann's constant = 1.380658×10^{-23} Joules/K. The quantity ν is the wavenumber (cm^{-1}) and $B(\nu,T)$ represents the blackbody spectral radiance per unit wavenumber.

The Rayleigh-Jeans approximation can be obtained from Equation (2) if $(ch\nu/kT) \ll 1$,

$$B(\nu, T) = 2kc\nu^2 T \qquad (3)$$

Equation (3) defines a brightness temperature $T_B = B(\nu,T_B)/(2kc\nu^2)$, which is an equivalent blackbody temperature.

The Planck function in Equation (2) gives the radiance from two orthogonal polarizations of unpolarized atmospheric radiation. Since the AMSU-A antenna is polarized, it will only detect half of the power incident upon its surface. Hence, a factor of ½ should be introduced in calculation of the detected power [5]. On the other hand, the factor 2 should be restored in the retrieval process and Equation (2) be used for obtaining the brightness temperature of the

radiating media. To simplify application, Equation (2) can be written as

$$B(\nu,T) = \frac{C_1 \nu^3}{\exp\left(C_2 \frac{\nu}{T}\right) - 1} \tag{4}$$

where the new constants C_1 and C_2 are given by $C_1 = 2hc^2 = 1.191044 \times 10^{-2}$ μW/(m^2-sr-cm^{-4}), and $C_2 = ch/k = 1.438769$ K/cm^{-1}. It is convenient to use the unit of μW (i.e., 10^{-6} Watts) for representing the radiance in the AMSU-A spectral region. The PRT temperatures T_s, T_c, and T_w from the scene, cold, and warm calibration targets were converted into radiances, R_s, R_c, and R_w, respectively, using Equation (4). We shall refer to the quantities R_x (where x=s, c or w) as the "PRT radiances."

3. CALIBRATION ALGORITHM

The goal of pre-launch calibration is to find a good analytic representation that can reproduce the measured PRT scene radiance. The scene target-view radiance, which corresponds to R_s, can be obtained from the radiometric counts and the PRT radiances R_c and R_w, using the calibration algorithm [6] which takes into account any nonlinear contribution due to an imperfect square law detector,

$$R_s = R_w + (R_w - R_c)\left(\frac{C_s - C_w}{C_w - C_c}\right) + \mu(R_w - R_c)^2 \left[\frac{(C_s - C_c)(C_s - C_w)}{(C_w - C_c)^2}\right] \tag{5}$$

where C_s, C_c, and C_w are the radiometric counts from the scene, cold, and warm targets, respectively. The first two terms in Equation (5) represent the linear contribution. The last term, which contains the nonlinear parameter μ, is attributed to an imperfect square-law detector. Equation (5) can be used for analyzing the AMSU-A EM calibration data.

First, we want to investigate the "calibration accuracy," which is defined in the document "Performance and Operation Specification for the AMSU-A" [7], as the difference (error) between the brightness temperature inferred from the microwave radiometer and the actual brightness temperature of a blackbody test target directly in front of the antenna. However, the "inferred" brightness temperature from the radiometer is undefined in [7]. Aerojet inferred this

quantity from the first two terms in Equation (5) with the R_w replaced by a modified $R_w' = R_w + R_{wo}$, where the quantity R_{wo} represents the difference between the radiometric radiance and the PRT radiance of the warm target. This is referred to as the "in-flight warm calibration target fixed bias correction" in [8]. A special set of calibration data, which were acquired by setting the variable scene-target temperature to the internal warm-target temperature [3], was used to obtain the R_{wo} values. In obtaining the radiometric warm-target radiance, the scene and cold targets were taken as the reference targets to provide two calibration points. Appendix A outlines how the quantity R_{wo} is determined. We define the calibration accuracy, ΔR, as the mean of differences between the measured PRT radiance of the scene target and its radiometric radiance obtained from the two linear terms in Equation (5). It is represented by the formula

$$\Delta R = \frac{1}{N} \sum_{n=1}^{N} (R_s - R_L)_n \tag{6}$$

where N=120 (3600) for A2 (A1) channels is the number of data samples and R_L represents the two linear terms in Equation (5) with the R_w replaced by the modified R_w',

$$R_L = R_w' + (R_w' - R_c)\left(\frac{C_s - C_w}{C_w - C_c}\right) \tag{7}$$

where

$$R_w' = R_w + R_{wo} \tag{8}$$

The warm target fixed bias correction factors R_{wo} were provided by Aerojet and are listed in Table 4 for all channels at five instrument temperature combinations. "Temperature Combination (TC)" represents a set of instrument (receiver shelf or RF shelf) temperature and the baseplate interface temperature used in the data acquisition. Since the latter was fixed at 15°C, only the former is listed in the plots and in Table 5 for each TC. It should be noted that the A1 data obtained with TC 6 (shaded area in Table 4) were waived (Waiver Number W013) due to large variations of receiver shelf temperature which deviated from predicted value. All data and parameter values related to this waived TC 6 dataset are shown in shaded areas in the following tables.

In Equation (7), the radiometric counts C_c and C_w are the average values of two samples. For the A1 channels (where the data were taken under the 10-10-10 Calibration Mode), the last two

samples of cold-target counts were used for the C_c average, and the first two samples of warm-target counts were used for the C_w average. Table 3 shows that ten cold- and warm-target samples are available, but eight of the data samples (in shaded areas) are not used. This selection of cold and warm calibration samples closely resembles the actual orbital scenario in space and allows for ten scene-target samples being used in the calculations.

4. RESULTS

Figures 1 through 8 show the plots of the calculated calibration accuracies for channels 1 through 15. The quantities along the ordinates on the left-hand side of these plots represent the calculated ΔR values from Equation (6) while the corresponding values in brightness temperature, ΔT (K), are shown on the right-hand side. The PRT scene radiances, R_s, which correspond to 84K (the lowest data point) to 330 K (the highest data point) in brightness temperature, are plotted along the abscissas. On the top of each figure, the required instrument specification for each channel is also listed. The specification requires $\Delta T = 2.0K$ for channels 1, 2, and 15, and $\Delta T = 1.5K$ for all other channels.

For each channel, three different plots are presented in Figures 1 to 8. The plot at the top in each figure was generated from the calibration data obtained with the primary phase locked loop oscillator (PLLO) using 25K scene-target temperature steps, whereas the one in the middle was produced from data acquired at 50K scene-target temperature steps using the secondary (redundant) PLLO. The plot at the bottom is the same as that on the top, except 50K steps of scene-target temperature were used in taking the data. In the EM calibration, both 25K- and 50K-step data were taken and used to test whether the two sets of data would produce same values of the nonlinearity parameter μ. If it is the same, then the calibration data will be done only at 50K steps for the AMSU-A Protoflight and Flight Models. However, it will be shown later that the μ values obtained from least-squares fit to the 25K- and 50K-steps data can be different.

The different curves shown in Figures 1-8 correspond to different instrument (RF Shelf) temperatures, which are also listed in the figures. These instrument temperatures are the mean values of the instrument temperatures, which were measured during the data collection periods. The instrument temperature was stabilized within $\pm 1^{\circ}C$ at each scene temperature, but these stabilized values could differ (by several degrees) as the scene-target temperature changes from 84K to 330K.

The ΔT values in Figures 1 through 8 are less than 0.5K and the ΔR-R_s curves show two

different shapes. The shapes shown in Figures 1, 3, 5, and 6 (channels 1, 2, 5, 8, and 9-12) are "parabolas," which can be approximately simulated by the quadratic term in Equation (5). The others (Figures 2, 4, 7, and 8) have a "linear" relationship with respect to the PRT scene radiances. It should be noted that the last term in Equation (5) also contains a linear component in $(C_s - C_w)$ if one expands the product. This will be discussed in Appendix B.

Next, we perform a least-squares analysis of the ΔR versus R_s curves in Figures 1 through 8. To a first-order approximation, the radiometric counts are proportional to the PRT radiances of individual targets so that we can express the quadratic term in Equation (5) as (note that R_w is replaced by R_w'),

$$Q = \mu\left(R_w' - R_c\right)^2\left[\frac{(C_s - C_c)(C_s - C_w)}{(C_w - C_c)^2}\right] = \mu\left(R_s - R_c\right)\left(R_s - R_w'\right) \qquad \textbf{(9)}$$

Equation (9) is simply a quadratic equation in R_s with zero error at $R_s = R_c$ and R_w'. One can determine the parameter μ from the least-squares fit formula,

$$\mu = \frac{\sum_{i=1}^{n} Q_i\left[\left(R_s - R_c\right)\left(R_s - R_w'\right)\right]_i}{\sum_{i=1}^{n}\left[\left(R_s - R_c\right)\left(R_s - R_w'\right)\right]_i^2} \qquad \textbf{(10)}$$

where $Q_i = (\Delta R)_i$ and n denotes the number of data points for each curve, as shown in Figures 1 to 8. In the cases of Cycle 1 curves, n equals 11; whereas in cases of Cycles 2 and 3, n is 6. If there are missing (or bad) data, n is reduced accordingly.

The best-fit μ values for all channels and different instrument temperatures are listed in Table 5. The values in the shaded areas are related to the waived TC 6 data and should be disregarded (the same for all following tables). Using these best-fit μ values, one can calculate the quadratic contributions from the right-hand side of Equation (9). Figures 9 through 16 show the plots of the residuals of the calibration accuracies after subtracting the best-fit Q values from the ΔR values (Figures 1 to 8). Comparison between the group of curves in Figures 9 - 16 and the corresponding ones in Figures 1 - 8 shows that the ΔR values for channels 1, 2, 5, 8, 9, 10, 11, and 12 are reduced considerably after applying the quadratic fits. On the other hand, there are no significant changes in other channels. Further discussion of improvement in fits to these

channels is given in Appendix B.

From Equation (9), one can show that the maximum value of Q occurs at $R_s=(R_w' + R_c)/2$. Substituting this value into Equation (9), one obtains the absolute maximum Q values in terms of R_w' and R_c

$$Q_{\max} = -\frac{1}{4}\mu\left(R_w' - R_c\right)^2 \tag{11}$$

Using the μ values in Table 5, one can calculate the Q_{max} values for each of the curves in Figures 1-8. Table 6 lists these calculated Q_{max} values.

Each of the curves in Figures 1-8 (Figures 9-16) can be characterized by the mean value and standard deviation of the calibration accuracies (the residuals after applying the quadratic fits). Table 7 lists the calculated mean values and standard deviations for each curve in Figures 1 through 16. For each instrument temperature (identified by the AMSU-A File ID in the fourth and last columns; also see Table 5), the first row (labeled by mL in column 1) lists the mean values of the calibration accuracy for each curve in Figures 1 through 8; while the second row (labeled as $\sigma 1$ in column 1) gives the standard deviations of each curve in Figures 1-8. Similarly, the third row (labeled as mQ) and fourth row (labeled as $\sigma 2$) list the mean values and standard deviations of the residuals after applying the quadratic fits (Figures 9-16). Table 7 shows that most of the absolute mean values and standard deviations are less than 0.1K and that the magnitude of the mean value is of the same order as the standard deviation for each curve. For the parabolic curves, the standard deviations are reduced considerably after applying the quadratic fits. For example, the standard deviations for channels 5 and 8 are approximately reduced by a factor of 4 after subtracting the quadratic fits from the calibration accuracies. However, there is little change in the linear cases.

The radiometric temperature sensitivity, NEΔT, is defined as the minimum detectable change of the brightness temperature incident at the antenna collecting aperture [7]. The limit of the radiometric temperature sensitivity only depends on electronic noise ($NE\Delta T \approx T_{sys}/\sqrt{B\tau}$, where τ=0.165 second for A1 and 0.158 second for A2 is the scene integration time, B is the predetection bandwidth, and T_{sys} is the system noise temperature). Its value, which can only be detected when all other noise sources are minimized, is calculated as the standard deviation of the radiometer outputs in degrees Kelvin (K) when the antenna is viewing a 300K uniform target. We calculated the NEΔT values from the calibration data (Cycle 1 and instrument

temperature = 26.9°C, i.e., Temperature Combination 1) taken at the scene-target temperature T_s = 304.2K (which is the one closest to 300K). This is shown in Figure 17. In the bottom part of Figure 17, the calculated NEΔT values of the 15 channels are compared to the AMSU-A specifications [7]. One can see that the calculated NEΔT values are less than the specifications, except those at channels 9 and 15, which exceed the required specifications of 0.25K and 0.5K, respectively, for these two channels. The two calculated NEΔT values are 0.34K and 0.52K. However, Aerojet determined that the large NEΔT value at channel 9 was due to un-optimized mixer and its requirement for EM was waived (Waiver Number W010). The NEΔT value in the other case exceeds the limit by a small margin and probably meets the requirement within measurement uncertainty.

The NEΔT values can be reduced by averaging the cold- and warm-target calibration measurements over several scans. The effect of averaging over the number of scans on the NEΔT values is demonstrated in the upper part of Figure 17, which shows the calculated NEΔT values of channels 1 and 2 as a function of the number of scans used in the averaging process. The results in this figure were obtained by using the running averages of all quantities on the right-hand side of Equation (7), except the scene-target count C_s, which is not averaged. Figure 17 shows that the NEΔT values gradually decrease as the number of scans increases from N_s=1 to 3, and then remain approximately constant. Results for other channels show similar features. This indicates that one can use this averaging process to reduce the noise-equivalent temperature uncertainties. Since a total-power radiometer requires frequent calibration to account for its gain drift, the time interval of averaging over scans should be limited to one minute or less. This, in turn, puts a limit on $N_s \leq 7$ (corresponding 56 seconds) for the AMSU-A data processing. Thus, the number of scans which may be used in this averaging process falls in the range of N_s=4 to 7.

5. DISCUSSION AND CONCLUSION

The analysis of the AMSU-A EM calibration data yields many interesting results and provides us with a better understanding of the functioning of the instrument. Experience and information gained from this study will offer useful insights to our software development for NOAA-K,L,M data processing. Some of the main features of interest revealed in this study are discussed in this section.

The warm target fixed bias correction factor, R_{wo}, plays an important role in this analysis. Effect of the factor R_{wo} on the calibration accuracy is demonstrated in Figure 18. The plots in the upper part of Figure 18 were obtained without R_{wo} (i. e., R_{wo}=0.0) in the calculation of all

six curves, whereas those in the lower part (which is the same one shown in the upper-left part of Figure 1) were calculated with the warm load correction factor R_{wo} included. One can see that the differences between the two sets of results (at the high end of the PRT radiances) are more than 0.5K. The R_{wo} values for 15 channels and five different instrument temperatures (see Table 4) were provided by Aerojet. These R_{wo} values were determined by setting the variable scene-target temperature to the internal warm-target temperature [3] to acquire the calibration data, which were then used to compute the R_{wo} values as discussed in Appendix A. Since this special set of calibration data was not delivered to us, we could not compute the R_{wo} factors. An attempt was made to compute the R_{wo} factors using the calibration data taken at the scene-target temperatures T_s = 280K and 305K (corresponding to radiance values of 1.46 and 1.59 in channel 1), respectively, but the R_{wo} values so produced differ from those listed in Table 4. Figure 19 shows the results when the R_{wo} values computed with the calibration data at T_s= 280K are employed. One should note that all curves in Figure 19 cross the zero error line (the dotted lines) at T_s= 280K, instead of the internal warm-target temperatures, which lie between T_s= 280K and 305K. Comparing the results in Figures 19 and 1, one can easily see the different appearances around T_s= 280K (i.e., PRT radiance=1.46 and 2.54 at channels 1 and 2).

Since only linear terms are included in calculation of the R_{wo} values (see Appendix A), the factor R_{wo} (at least part of it) may be attributed to nonlinear contribution, instead of fixed bias correction. Perhaps, it would not be necessary to make this R_{wo} correction if the modified version of the quadratic term (see Appendix B) is used to fit the data.

Some of the curves in Figures 1 to 8 do not cross the zero error lines at the internal warm-target temperatures (e.g., the f curves in Figure 1). This suggests that the R_{wo} values (Table 4) corresponding to these curves may be incorrect. For the same reason, it seems that the cold target also needs a fixed bias correction. This can be seen from the sample data listed in Table 2. For example, the radiometric counts of scene target and cold target for channel 1 consistently differ by about 3 counts, even though the scene-target temperature and cold-target temperature (both measured by PRTs) are practically identical. Since the gain of this channel is 13.2 count/K, a difference of 3 counts would produce 0.23K in difference of brightness temperatures. This 0.23K approximately equals the cold target fixed bias correction for this case (Figure 1).

The 10-10-10 Calibration Mode is an ingenious method for collecting a large number of data samples in a short time period. However, the time series of the samples are not identical to the actual orbital scenario. Although ten samples from each warm and cold target were collected in each scan, only two of the samples (from each target) were used in the calibration. The data samples listed in Table 3 show large fluctuation among the ten samples collected in a single

scan. For example, the ten warm-target samples for channel 3 differ by 15 counts from the smallest to largest radiometric counts. This difference of 15 counts corresponds to 1K in temperature difference (the gain for this channel is 14.4 count/K). Even larger fluctuation occurs in samples of the warm-target counts at channel 14 (see Table 3). This indicates that the calibration results may depend upon which samples (two out of ten) are chosen.

The nonlinear parameter μ depends on instrument temperature. The instrument (RF Shelf) temperature can vary several degrees during a data-collection cycle when the scene-target temperature is varied from 84K to 330K. Table 8 shows one set of such instrument-temperature variation for AMSU-A1-1 channels. The RF Shelf temperature varies from 15.9°C to 18.9°C. These instrument temperatures were obtained from PRT counts, which were converted into temperatures from a count-to-temperature table supplied by Aerojet. The effect of such instrument-temperature variation on the μ parameter is unknown and is difficult to estimate.

The μ values (Table 5) for the parabolic curves (e.g., Channels 5 and 8) show some "regular" variations as a function of instrument temperature, whereas those for the linear ones do not show any regular pattern. Also, the μ values of Cycle 1 (25K-step data) differ from those of Cycle 3 (50K-step data). This will produce different results in radiance when the μ values are used in the calibration equation, particularly at the cold-space temperature region near T_s=2.73K. For example, the μ values for Cycle 1 (25K steps) and Cycle 3 (50K steps) at channels 1-2 and Temperature Combinations 2 and 4 (see Table 5) differ by large amounts, which would produce 0.08 to 0.17K differences in brightness temperature if the two sets of μ values are applied to compute the Q_{max} values.

One can see from Figures 9-16 that Equation (5) with one nonlinear parameter can reproduce the PRT scene radiances with residual errors up to about 0.4K. However, these residual errors can be reduced to about 0.1K if a modified version of the quadratic term with three nonlinear parameters (see Appendix B) is applied to fit the data. The achievement of 0.1K in the residual calibration error is particularly important for climatology studies, which seek a long-term trend of atmospheric temperature anomalies with a magnitude less than 1K.

ACKNOWLEDGEMENTS: The authors want to thank Wilfred Mazur, Jr. of NOAA/SPO for his support and for his persistent effort in providing the data and information. We are indebted to James Mentall and James Shiue of NASA/GSFC for technical discussions about the AMSU-A instruments. One of us (T. M.) is indebted to P. K. Patel, J. Frey and R. V. Hauerwaas of Aerojet, and to S. Krimchansky of NASA/GSFC for their assistance in processing the data.

REFERENCES

[1]. "Notes for Processing AMSU-A Calibration Data," T. Mo, 1993 (in preparation).

[2]. PRT Handbook, Bulletin 1042, 1986, Rosemount Inc., Burnsville, MN 55337.

[3]. "AMSU-A Calibration Process Flow." J. Frey and P. Patel, Aerojet, Report No. 10186, March 1993.

[4]. "The Fundamental Physical Constants," E. R. Cohen and B. N. Taylor, Physics Today, PP. BG9 - 13, August 1992; Rev. Mod. Phys. vol. 57, p. 1121, 1987.

[5]. Microwave Remote Sensing, Vol. 1, F. T. Ulaby, R. K. Moore, and A. K. Fung, (P. 189), Addison-Wesley, 1981

[6]. "Advanced Microwave Sounding Unit-A (AMSU-A), " Vol 1 - Technical Proposal, February 1985, P9112-80-02, Aerojet, Azusa, CA 91702.

[7]. "Performance and Operation Specification for the AMSU-A," Contract Attachment B, S-480-13, NASA/GSFC, August 1984.

[8]. "System Calibration Test Procedure for the AMSU-A1 System," February 1992, AE-26156/5, Aerojet, Azusa, CA 91702.

APPENDIX A

The in-flight warm calibration target fixed bias correction was calculated by Aerojet [8] from a special set of calibration data, which were acquired by setting the variable scene-target temperature to the internal warm-target temperature. The physical temperature T_w of internal warm target was determined by PRTs. The in-flight warm load radiometric temperature T_{wrad} was obtained for each scan by the formula

$$T_{wrad} = T_s + (T_s - T_c)\left(\frac{C_w - C_s}{C_s - C_c}\right) \qquad \text{(A-1)}$$

where:
T_s = PRT temperature of the variable scene target,
T_c = PRT temperature of the fixed cold target,
C_w = the average of two radiometric counts from the warm target,
C_c = the average of two radiometric counts from the cold target, and
C_s = radiometric counts from the variable scene target.

The in-flight warm calibration target fixed bias correction factor T_{wo} was computed from the formula

$$T_{wo} = \frac{1}{N}\sum_{i=1}^{N}(T_{wrad} - T_w)_i \qquad \text{(A-2)}$$

where N represents the number of data samples. The T_{wo} values (in K) are listed in Table 4 and are converted into radiances, R_{wo}, which are used in this study.

APPENDIX B

It is easy to show that the quadratic term in Equation (5) (or Equation 9) can be written in the form,

$$Q = \mu\left(R_w' - R_c\right)^2\left[\frac{\left(C_s - C_w\right)^2}{\left(C_w - C_c\right)^2} + \frac{\left(C_s - C_w\right)}{\left(C_w - C_c\right)}\right] \qquad \text{(B-1)}$$

The second term in the bracket is linear in $(C_s - C_w)$. To account for the fact that some of the ΔR values (see Figures 1 - 8) show a linear relationship with respect to the scene radiance R_s, we can add a constant term into the bracket in Equation (B-1) and use it to fit the curves in Figures 1 to 8. Equation (B-1) is then written as

$$Q = \mu_0\left(R_w' - R_c\right)^2 + \mu_1\left(R_w' - R_c\right)^2\left(\frac{C_s - C_w}{C_w - C_c}\right) + \mu_2\left(R_w' - R_c\right)^2\frac{\left(C_s - C_w\right)^2}{\left(C_w - C_c\right)^2} \qquad \text{(B-2)}$$

As in the case of Equation (9), the transformation of Equation (B-2) in terms of radiances becomes

$$Q = \mu_0\left(R_w' - R_c\right)^2 + \mu_1\left(R_w' - R_c\right)\left(R_s - R_w'\right) + \mu_2\left(R_s - R_w'\right)^2 \qquad \text{(B-3)}$$

where μ_0, μ_1, and μ_2 are taken as free parameters which can be determined by least-squares fits to curves in Figures 1 - 8. The first term in Equation (B-3) is the newly added term, which corresponds to a constant term, since the quantity $(R_w' - R_c)$ is approximately constant for a set of calibration data as shown in each of the curves. The first term in Equation (B-3) may be attributed to some undetermined relative biases among the blackbody targets.

For fitting the parabolic curves in Figures 1-8 with Equation (B-3), one would expect μ_0 being very small (or close to zero), while in the cases of linear ones, μ_2 should be relatively small. After the nonlinearity parameters are determined, one can use Equation (B-2) to compute the Q values. Figure B-1 shows a sample of best-fit results obtained with Equation (B-3). It should be compared with those shown in the upper part of Figure 16. One can see that the residual errors are reduced to less than 0.1K.

Table 1. AMSU-A channel characteristics and specifications.

CH. NO.	CENTER FREQUENCY (MHz)	NO. OF PASS BANDS	BANDWIDTH (MHz)	TEMPERATURE SENSITIVITY (K)	CALIBRATION ACCURACY (K)
1	23800	1	270	0.3	2.0
2	31400	1	180	0.3	2.0
3	50300	1	180	0.4	1.5
4	52800	1	400	0.25	1.5
5	53596 ± 115	2	170	0.25	1.5
6	54400	1	400	0.25	1.5
7	54940	1	400	0.25	1.5
8	55500	1	330	0.25	1.5
9	57290.344	1	330	0.25	1.5
10	57290.344 ± 217	2	78	0.4	1.5
11	57290.344 ± 322.2 ± 48	4	36	0.4	1.5
12	57290.344 ± 322.2 ± 22	4	16	0.6	1.5
13	57290.344 ± 322.2 ± 10	4	8	0.8	1.5
14	57290.344 ± 322.2 ± 4.5	4	3	1.2	1.5
15	89000	1	6000	0.5	2.0

Table 2. Samples of AMSU-A2 Engineering Model Calibration Data* for Channels 1 and 2.

Scan No.	Time hh:mm:ss	Scene Temp. (K)	Warm Temp. (K)	Cold Temp. (K)	Ch. 1 Scene Count	Ch. 1 Warm Count	Ch. 1 Cold Count	Ch. 2 Scene Count	Ch. 2 Warm Count	Ch. 2 Cold Count
1	17:39:17	84.00	301.34	83.98	13409	16287	13411	12810	16019	12816
2	17:39:25	84.00	301.36	83.99	13407	16289	13411	12812	16019	12813
3	17:39:33	84.00	301.34	83.99	13405	16288	13412	12812	16022	12814
4	17:39:41	84.00	301.33	83.99	13408	16289	13412	12815	16022	12813
5	17:39:49	83.99	301.32	83.99	13408	16289	13414	12811	16019	12813
6	17:39:57	84.00	301.34	83.99	13404	16288	13411	12813	16020	12814
7	17:40:05	84.00	301.32	83.98	13409	16288	13413	12812	16019	12815
8	17:40:13	84.00	301.33	83.99	13408	16287	13410	12813	16020	12813
9	17:40:21	84.00	301.33	83.98	13409	16289	13410	12809	16019	12812
10	17:40:29	84.00	301.33	83.98	13408	16290	13410	12813	16022	12810
11	17:40:37	84.00	301.35	83.98	13410	16291	13412	12811	16018	12814
12	17:40:45	83.99	301.32	83.98	13408	16282	13411	12811	16017	12811
13	17:40:53	84.00	301.31	83.99	13408	16286	13410	12810	16016	12814
14	17:41:01	84.00	301.33	83.99	13411	16287	13408	12810	16018	12813
15	17:41:09	84.00	301.34	83.98	13410	16287	13407	12810	16019	12812
16	17:41:17	84.00	301.33	83.98	13407	16285	13410	12810	16022	12813
17	17:41:25	83.99	301.35	83.98	13407	16286	13410	12812	16019	12812
18	17:41:33	84.00	301.33	83.98	13409	16284	13410	12808	16018	12815
19	17:41:41	84.00	301.31	83.98	13410	16288	13411	12809	16022	12813
20	17:41:49	84.00	301.31	83.98	13410	16286	13411	12811	16018	12813
21	17:41:57	84.00	301.31	83.98	13409	16287	13410	12817	16019	12814
22	17:42:05	83.99	301.32	83.98	13408	16287	13411	12814	16019	12812
23	17:42:13	84.00	301.32	83.98	13410	16288	13410	12810	16019	12815
24	17:42:21	84.00	301.32	83.97	13407	16291	13411	12812	16023	12814
25	17:42:29	84.00	301.33	83.98	13411	16288	13409	12811	16020	12814
26	17:42:37	84.00	301.31	83.97	13408	16287	13410	12815	16023	12814
27	17:42:45	84.00	301.32	83.98	13410	16287	13411	12812	16020	12815
28	17:42:53	84.00	301.32	83.98	13407	16285	13408	12810	16022	12815
29	17:43:01	84.00	301.30	83.99	13406	16288	13411	12811	16020	12816
30	17:43:09	84.00	301.31	83.99	13409	16288	13411	12810	16020	12813

* 16-MAR-91, Data ID = A2_02_CYCLE1_SUB1_T084_B15_A40_O.DAT, GSE_TEST_MODE= 0 (Full Scan).

Table 3. Samples of AMSU-A1 EM calibration data* taken under the 10-10-10 Mode. All data were taken within one scan period of 8 seconds.

A1-2 Channels: Scene Temp.=304.35K, Warm Temp.=290.01K, Cold Temp.=83.92K

CH. NO.	TEN SAMPLES										TARGET ID
	1	2	3	4	5	6	7	8	9	10	
3	15654	15648	15649	15645	15654	15647	15654	15644	15643	15643	SCENE
4	16578	16577	16579	16580	16583	16576	16577	16582	16574	16582	
5	18255	18255	18251	18255	18251	18245	18256	18248	18253	18254	
8	18912	18906	18907	18903	18906	18905	18903	18909	18900	18904	
3	12464	12464	12468	12466	12466	12464	12466	12467	12463	12468	COLD
4	11440	11433	11441	11437	11438	11440	11436	11439	11442	11435	
5	13731	13736	13736	13735	13736	13738	13737	13736	13737	13734	
8	13794	13793	13789	13796	13790	13795	13795	13789	13790	13790	
3	15439	15442	15450	15435	15442	15441	15437	15440	15445	15436	WARM
4	16244	16247	16247	16245	16242	16249	16248	16251	16251	16246	
5	17962	17961	17962	17966	17962	17964	17961	17958	17964	17963	
8	18574	18575	18569	18571	18578	18575	18582	18570	18576	18576	

A1- 1 Channels : Scene Temp.=304.41K, Warm Temp.=281.46K, Cold Temp.=83.96K

6	16345	16344	16340	16345	16346	16342	16345	16347	16344	16345	SCENE
7	16524	16525	16525	16528	16524	16526	16523	16526	16523	16526	
9	17278	17282	17280	17280	17280	17278	17283	17279	17278	17282	
10	17539	17545	17547	17539	17544	17540	17540	17549	17545	17539	
11	18912	18920	18918	18918	18920	18921	18920	18921	18916	18915	
12	19355	19344	19348	19350	19368	19351	19354	19339	19344	19352	
13	19367	19375	19369	19362	19353	19351	19341	19351	19377	19340	
14	20362	20379	20369	20381	20361	20349	20374	20333	20381	20386	
15	15201	15202	15204	15203	15201	15203	15201	15201	15204	15202	
6	13641	13640	13636	13641	13643	13643	13642	13641	13644	13642	COLD
7	13774	13774	13778	13777	13777	13775	13776	13773	13774	13774	
9	15047	15047	15050	15050	15043	15043	15052	15049	15046	15046	
10	14876	14882	14878	14880	14881	14879	14876	14881	14887	14881	
11	15890	15890	15893	15892	15895	15892	15887	15891	15895	15888	
12	16285	16279	16282	16286	16287	16292	16298	16292	16296	16290	
13	16283	16284	16292	16289	16282	16281	16283	16279	16293	16288	
14	16964	16981	16977	16970	16967	16977	16997	16981	16984	16977	
15	14260	14261	14259	14263	14262	14264	14261	14261	14261	14263	
6	16066	16063	16066	16067	16063	16065	16066	16065	16065	16062	WARM
7	16240	16243	16239	16238	16245	16243	16242	16240	16240	16241	
9	17055	17048	17054	17051	17050	17051	17056	17053	17049	17052	
10	17270	17268	17270	17269	17269	17268	17268	17279	17271	17268	
11	18609	18605	18606	18610	18604	18603	18603	18604	18606	18602	
12	19042	19040	19034	19040	19033	19032	19043	19033	19042	19036	
13	19057	19035	19033	19037	19047	19052	19043	19031	19048	19033	
14	20024	20006	20020	20076	20002	20012	20014	20017	20008	20026	
15	15105	15106	15105	15106	15102	15106	15106	15106	15104	15105	

*** DATA FILE ID=A1_01_CYCLE1_SUB5_T305_B15_A20_C.DAT;1, 6-JUL-91, 17:53:31**

Note : Samples in the shaded areas were not used in the calculations

Table 4. Warm target fixed bias correction factors (in K)

Cycles 1 and 3 : (supplied by Aerojet)

Ch. No.	Temperature Combination				
	1	2	4	6*	7
1	-0.553	-0.588	-0.689	-0.494	-0.387
2	-0.422	-0.471	-0.592	-0.370	-0.324
3	0.067	0.076	0.114	0.143	-0.010
4	0.094	0.067	0.104	0.145	-0.001
5	0.085	0.078	0.103	0.138	-0.011
6	0.115	0.138	0.184	0.281	0.217
7	0.111	0.123	0.178	0.060	0.117
8	0.079	0.076	0.102	0.159	-0.015
9	0.223	0.316	0.334	0.024	0.191
10	0.039	0.065	0.156	0.063	0.142
11	0.137	0.126	0.159	0.031	-0.029
12	0.225	0.327	0.411	0.018	0.329
13	0.264	0.337	0.414	0.034	0.339
14	0.280	0.314	0.397	0.054	0.330
15	0.056	0.087	0.188	0.091	0.172

Cycle 2 : (supplied by Aerojet)

Ch. No.	Temperature Combination				
	1	2	4	6	7
1	-0.553	-0.588	-0.689	-0.494	-0.387
2	-0.422	-0.471	-0.592	-0.370	-0.324
3	0.043	0.090	0.380	0.156	-0.057
4	0.054	0.089	0.043	0.175	-0.073
5	0.058	0.091	0.043	0.159	-0.073
6	-0.068	0.170	0.187	0.305	-0.013
7	-0.091	0.152	0.148	0.086	-0.051
8	0.063	0.093	0.036	0.173	-0.075
9	-0.235	0.130	0.163	0.101	-0.029
10	-0.100	0.107	0.131	0.107	-0.016
11	-0.045	0.132	0.116	0.078	-0.164
12	-0.011	0.090	0.124	0.038	**
13	0.128	0.305	0.440	0.005	**
14	0.128	0.445	0.468	-0.011	-0.080
15	-0.088	0.166	0.166	0.096	-0.128

* **Data were waived** ** **= Bad Data**

Table 5. Best- fit values of the quadratic parameter μ [(m^2-sr-cm^-1)/μW]. Instrument temperautres are given in parenthesis in the first column.

AMSU-A2 CHANNELS:				AMSU-A1-2 CHANNELS:					
Temperature Combination	CH. 1	CH. 2	*AMSU-A2* Cycle/Sub	Temperature Combination	CH. 3	CH. 4	CH. 5	CH. 8	AMSU-A1-2 Cycle/Sub
1 (23.6C)#	4.3327E-04	1.7400E-03	C1S1	1 (26.9C)#	1.3753E-04	-2.2708E-04	1.4914E-03	1.0057E-03	C1S5
2 (19.0)	1.8666E-04	1.2845E-03	C1S2	2 (19.4)	-3.2969E-05	-3.6613E-04	1.3568E-03	8.7729E-04	C1S2
4 (14.0)	3.4031E-03	2.6472E-03	C1S3	4 (16.3)	-7.5353E-05	-4.1001E-04	1.4185E-03	9.2590E-04	C1S3
6 (8.8)	2.0243E-03	2.2148E-03	C1S5	6* (14.8)	-9.2356E-05	-7.3699E-04	1.1949E-03	6.7264E-04	C1S1
7 (6.1)	-1.0013E-03	8.8804E-04	C1S6	7 (6.7)	-1.1189E-04	-3.1250E-04	1.2539E-03	9.0111E-04	C1S6
4 (17.3)	2.0606E-03	1.9376E-03	C1S4	4 (17.0)	-1.0166E-04	-4.1786E-04	1.3767E-03	8.9689E-04	C1S4
1 (23.6C)	1.4669E-03	1.8773E-03	C2S1	1 (26.9C)	5.1834E-05	-2.8032E-04	1.4447E-03	9.5653E-04	C2S5
2 (19.0)	2.0127E-03	2.1865E-03	C2S2	2 (19.4)	-5.0366E-05	-3.2547E-04	1.3199E-03	8.6658E-04	C2S2
4 (14.0)	5.0145E-03	3.4164E-03	C2S3	4 (16.3)	-2.2872E-04	-2.1662E-04	1.3097E-03	8.4845E-04	C2S3
6 (8.8)	2.6937E-03	2.6689E-03	C2S4	6* (14.8)	3.9762E-04	-2.6581E-04	1.4942E-03	1.0160E-03	C2S1
7 (6.1)	-1.8746E-03	3.5358E-04	C2S5	7 (6.7)	2.1896E-04	-1.2556E-04	1.3978E-03	1.0103E-03	C2S6
1 (23.6C)	1.4244E-03	1.9846E-03	C3S1	1 (26.9C)	7.4438E-06	-3.6074E-04	1.3323E-03	8.3446E-04	C3S5
2 (19.0)	3.0903E-03	2.9357E-03	C3S2	2 (19.4)	-1.3158E-04	-4.0756E-04	1.2395E-03	7.7785E-04	C3S2
4 (14.0)	4.8201E-03	3.8093E-03	C3S3	4 (16.3)	7.6714E-05	-2.5185E-04	1.4266E-03	9.3557E-04	C3S3
6 (8.8)	3.0160E-03	2.6122E-03	C3S4	6* (14.8)	8.7459E-05	-5.3935E-04	1.2450E-03	7.4033E-04	C3S1
7 (6.1)	-1.0351E-03	1.1694E-03	C3S5	7 (6.7)	2.1541E-05	-2.8128E-04	1.2083E-03	8.9828E-04	C3S6

AMSU-A1-1 CHANNELS:										
Temperature Combination	CH. 6	CH. 7	CH. 9	CH. 10	CH. 11	CH. 12	CH. 13	CH. 14	CH. 15	AMSU-A1-1 Cycle/Sub
1 (25.2C)#	2.3798E-04	-2.5431E-04	5.2099E-04	3.6303E-04	5.8615E-04	4.5686E-04	3.2867E-04	1.1890E-04	-5.2295E-05	C1S5
2 (17.2)	2.0919E-04	-2.1342E-04	4.9352E-04	2.7113E-04	7.0383E-04	5.4353E-04	3.7823E-04	2.0307E-04	-6.1934E-05	C1S2
4 (14.1)	1.9268E-04	-2.3382E-04	5.0482E-04	2.0985E-04	7.6501E-04	6.7402E-04	5.4400E-04	3.0043E-04	-4.8522E-05	C1S3
6* (15.3)	1.2680E-04	-2.7090E-04	4.9811E-04	3.1449E-04	5.9694E-04	5.4815E-04	5.0137E-04	2.1402E-04	-1.4188E-04	C1S1
7 (3.8)	-1.6851E-05	-2.6398E-04	3.9869E-04	9.7844E-05	4.4384E-04	7.3515E-04	5.2816E-04	3.3908E-04	-1.3000E-04	C1S6
4 (16.0)	3.2196E-04	-1.1028E-04	6.1024E-04	3.4374E-04	8.3360E-04	7.6133E-04	7.1506E-04	4.6815E-04	-1.4052E-07	C1S4
1 (25.2C)	2.9785E-04	-1.2543E-04	4.9884E-04	4.6147E-04	5.9509E-04	6.4924E-04	4.4442E-04	2.6641E-04	-7.9700E-05	C2S5
2 (17.2)	1.1736E-04	-2.3534E-04	4.5363E-04	3.2080E-04	5.3967E-04	7.1661E-04	6.9690E-04	4.4100E-04	-1.0208E-04	C2S2
4 (14.1)	1.0761E-04	-1.1646E-04	3.5102E-04	4.0041E-04	5.9912E-04	8.2373E-04	6.0267E-04	4.7124E-04	-7.0614E-05	C2S3
6* (15.3)	-2.1079E-04	-1.3895E-04	4.7600E-04	3.5875E-04	6.6648E-04	4.9392E-04	2.7088E-04	2.8964E-05	-7.3048E-05	C2S1
7 (3.8)	2.9611E-04	-5.0934E-05	4.9687E-04	4.1163E-04	7.7331E-04	**	**	**	2.3292E-06	C2S6
1 (25.2C)	2.0621E-04	-1.9468E-04	4.5006E-04	4.1187E-04	5.5388E-04	4.5142E-04	2.4856E-04	7.5342E-05	-6.6075E-05	C3S5
2 (17.2)	1.2972E-04	-2.3892E-04	4.2541E-04	2.2444E-04	6.4843E-04	5.5505E-04	3.3749E-04	1.1769E-04	-9.5223E-05	C3S2
4 (14.1)	2.0215E-04	-1.8999E-04	4.8142E-04	2.8461E-04	7.6260E-04	6.1517E-04	4.2632E-04	2.7469E-04	-6.9525E-05	C3S3
6* (15.3)	3.2476E-04	-8.8457E-05	5.8857E-04	4.2638E-04	7.6956E-04	6.8977E-04	5.8351E-04	2.5423E-04	-7.7577E-05	C3S1
7 (3.8)	9.9184E-05	-2.2281E-04	3.8423E-04	2.1053E-04	6.0019E-04	7.3820E-04	6.0676E-04	2.8431E-04	-9.8859E-05	C3S6

 # Instrument Temperature

*** Data in the shaded areas were waived**

**** = Bad Data**

Table 6. Maximum values (K) of the quadratic contribution calculated from Equation (11).

AMSU-A2 CHANNELS:				AMSU-A1 CHANNELS:												
Temperature Combination	CH. 1	CH. 2	AMSU-A2 Cycle/Sub	CH. 3	4	5	6	7	8	9	10	11	12	13	14	15	AMSU-A1 Cycle/Sub
1	-0.026	-0.180	C1S1	-0.034	0.062	-0.422	-0.065	0.071	-0.305	-0.158	-0.110	-0.178	-0.139	-0.100	-0.036	0.038	C1S5
2	-0.011	-0.129	C1S2	0.008	0.093	-0.356	-0.058	0.060	-0.247	-0.152	-0.083	-0.217	-0.167	-0.116	-0.062	0.046	C1S2
4	-0.183	-0.247	C1S3	0.017	0.100	-0.355	-0.051	0.063	-0.248	-0.148	-0.062	-0.225	-0.198	-0.160	-0.088	0.034	C1S3
6	-0.105	-0.199	C1S5	0.020	0.179	-0.299	-0.034	0.073	-0.181	-0.146	-0.092	-0.175	-0.161	-0.147	-0.063	0.100	C1S1*
7	0.050	-0.077	C1S6	0.023	0.070	-0.289	0.004	0.067	-0.222	-0.109	-0.027	-0.122	-0.202	-0.145	-0.093	0.086	C1S6
4	-0.111	-0.182	C1S4	0.023	0.105	-0.356	-0.088	0.031	-0.249	-0.186	-0.105	-0.254	-0.232	-0.218	-0.143	0.000	C1S4
1	-0.087	-0.193	C2S1	-0.013	0.078	-0.413	-0.084	0.036	-0.293	-0.156	-0.144	-0.186	-0.203	-0.139	-0.083	0.060	C2S5
2	-0.116	-0.218	C2S2	0.012	0.082	-0.343	-0.032	0.066	-0.242	-0.138	-0.098	-0.164	-0.218	-0.212	-0.134	0.075	C2S2
4	-0.270	-0.320	C2S3	0.051	0.053	-0.330	-0.029	0.032	-0.229	-0.104	-0.118	-0.177	-0.244	-0.178	-0.139	0.050	C2S3
6	-0.138	-0.237	C2S4	-0.087	0.064	-0.372	0.055	0.037	-0.271	-0.137	-0.103	-0.191	-0.142	-0.078	-0.008	0.051	C2S1*
7	0.091	-0.030	C2S5	-0.044	0.028	-0.321	-0.073	0.013	-0.249	-0.136	-0.112	-0.211	**	**	**	-0.002	C2S6
1	-0.084	-0.203	C3S1	-0.002	0.098	-0.373	-0.055	0.053	-0.250	-0.133	-0.121	-0.163	-0.133	-0.073	-0.022	0.047	C3S5
2	-0.178	-0.294	C3S2	0.030	0.103	-0.321	-0.035	0.067	-0.216	-0.129	-0.068	-0.196	-0.168	-0.102	-0.036	0.070	C3S2
4	-0.260	-0.358	C3S3	-0.017	0.061	-0.356	-0.053	0.051	-0.250	-0.141	-0.083	-0.223	-0.180	-0.125	-0.080	0.049	C3S3
6	-0.156	-0.235	C3S4	-0.019	0.131	-0.312	-0.086	0.024	-0.199	-0.173	-0.125	-0.226	-0.203	-0.171	-0.075	0.055	C3S1*
7	0.050	-0.099	C3S5	-0.004	0.062	-0.277	-0.024	0.056	-0.220	-0.105	-0.057	-0.163	-0.201	-0.165	-0.077	0.065	C3S6

*** Data in the shaded areas were waived** **** = Bad Data**

Specification: 0.50 K for Ch. 1, 2 and 15,
0.375K for Ch. 3 to 14.

Table 7. Mean values and standard deviations of calibration accuracy and residuals of the quadratic fits.

Mean/ STD Dev.	Ch. 1 (K)	Ch. 2 (K)	AMSU-A2 FILE ID	Ch.3 (K)	Ch. 4 (K)	Ch.5 (K)	Ch. 6 (K)	Ch. 7 (K)	Ch. 8 (K)	Ch. 9 (K)	Ch. 10 (K)	Ch. 11 (K)	Ch. 12 (K)	Ch. 13 (K)	Ch. 14 (K)	Ch. 15 (K)	AMSU-A1 File ID
mL	0.02	-0.07	C1S1	0.00	0.05	-0.18	-0.03	0.07	-0.13	-0.06	0.00	-0.05	-0.02	0.00	-0.02	-0.01	S1C5
σ1	0.07	0.13		0.05	0.06	0.24	0.07	0.05	0.17	0.11	0.09	0.12	0.10	0.09	0.04	0.09	
mQ	0.03	0.01		0.02	0.03	-0.02	-0.02	0.05	-0.02	-0.02	0.03	-0.01	0.01	0.03	-0.01	-0.02	
σ2	0.07	0.07		0.04	0.06	0.06	0.06	0.06	0.04	0.07	0.04	0.04	0.04	0.05	0.03	0.08	
mL	0.04	-0.01	C1S2	0.02	0.06	-0.13	-0.05	0.04	-0.10	-0.09	-0.02	-0.09	-0.08	-0.07	-0.03	-0.01	S1C2
σ1	0.08	0.12		0.04	0.07	0.23	0.05	0.07	0.16	0.08	0.07	0.13	0.10	0.07	0.05	0.11	
mQ	0.05	0.04		0.02	0.03	-0.02	-0.03	0.02	-0.02	-0.04	0.01	-0.02	-0.03	-0.03	-0.01	-0.02	
σ2	0.07	0.07		0.04	0.05	0.05	0.05	0.06	0.03	0.04	0.04	0.05	0.03	0.04	0.04	0.10	
mL	-0.10	-0.10	C1S3	0.02	0.07	-0.18	-0.04	0.04	-0.12	-0.10	-0.02	-0.12	-0.12	-0.10	-0.07	0.01	S1C3
σ1	0.13	0.17		0.04	0.06	0.17	0.05	0.05	0.12	0.08	0.06	0.10	0.09	0.06	0.06	0.08	
mQ	-0.03	-0.02		0.02	0.02	-0.02	-0.01	0.01	-0.01	-0.03	0.01	-0.01	-0.03	-0.03	-0.03	0.00	
σ2	0.09	0.08		0.04	0.05	0.05	0.05	0.05	0.04	0.07	0.04	0.03	0.05	0.05	0.06	0.08	
mL	-0.02	-0.06	C1S4	-0.01	0.09	-0.13	0.01	0.06	-0.09	-0.06	-0.01	-0.05	-0.05	-0.06	-0.03	0.03	**S1C1***
σ1	0.11	0.13		0.06	0.15	0.20	0.05	0.05	0.12	0.11	0.08	0.15	0.14	0.12	0.09	0.11	
mQ	0.03	0.03		-0.02	0.04	-0.05	0.02	0.04	-0.04	-0.02	0.01	0.00	0.00	-0.02	-0.01	0.00	
σ2	0.07	0.07		0.05	0.11	0.06	0.05	0.04	0.05	0.07	0.04	0.08	0.08	0.08	0.08	0.08	
mL	-0.03	-0.07	C1S5	0.11	0.11	0.00	0.00	0.05	0.02	-0.03	0.03	0.04	-0.05	-0.06	-0.04	0.00	S1C6
σ1	0.10	0.15		0.07	0.07	0.28	0.05	0.07	0.23	0.10	0.07	0.15	0.17	0.12	0.09	0.11	
mQ	0.01	-0.01		0.10	0.10	0.05	0.00	0.03	0.06	0.00	0.03	0.07	0.00	-0.02	-0.02	-0.03	
σ2	0.06	0.08		0.07	0.07	0.10	0.05	0.06	0.09	0.04	0.06	0.10	0.05	0.05	0.05	0.07	
mL	-0.09	-0.11	C1S6	-0.01	0.03	-0.20	-0.10	-0.02	-0.15	-0.16	-0.08	-0.17	-0.18	-0.18	-0.14	-0.06	S1C4
σ1	0.19	0.15		0.08	0.11	0.13	0.04	0.11	0.08	0.03	0.09	0.07	0.04	0.04	0.05	0.15	
mQ	-0.11	-0.09		-0.02	-0.01	-0.06	-0.07	-0.03	-0.05	-0.08	-0.04	-0.06	-0.09	-0.09	-0.07	-0.06	
σ2	0.17	0.16		0.08	0.09	0.07	0.07	0.10	0.06	0.08	0.10	0.08	0.10	0.10	0.09	0.15	
mL	0.01	-0.04	C2S1	0.04	0.08	-0.13	0.10	0.20	-0.09	0.09	0.11	0.07	0.07	0.04	0.07	0.11	C2S5
σ1	0.10	0.15		0.05	0.06	0.28	0.17	0.07	0.20	0.22	0.17	0.19	0.22	0.18	0.18	0.03	
mQ	0.04	0.03		0.05	0.06	-0.01	0.11	0.19	0.00	0.12	0.14	0.10	0.11	0.07	0.09	0.10	
σ2	0.06	0.07		0.05	0.06	0.07	0.15	0.09	0.05	0.16	0.10	0.10	0.13	0.13	0.16	0.05	
mL	0.01	-0.02	C2S2	-0.02	0.02	-0.12	-0.05	0.01	-0.10	-0.09	-0.05	-0.09	-0.11	-0.14	-0.07	-0.07	C2S2
σ1	0.12	0.18		0.03	0.08	0.29	0.02	0.08	0.20	0.10	0.08	0.13	0.17	0.17	0.12	0.13	
mQ	0.05	0.05		-0.02	0.00	-0.03	-0.04	-0.01	-0.03	-0.05	-0.02	-0.04	-0.05	-0.08	-0.03	-0.09	
σ2	0.06	0.06		0.03	0.03	0.05	0.02	0.06	0.04	0.03	0.04	0.04	0.03	0.10	0.07	0.10	
mL	-0.14	-0.11	C2S3	-0.19	0.06	-0.04	-0.04	0.02	-0.02	-0.06	0.00	-0.04	-0.13	-0.17	-0.09	-0.03	C2S3
σ1	0.18	0.23		0.19	0.07	0.30	0.06	0.05	0.21	0.10	0.11	0.15	0.24	0.21	0.19	0.10	
mQ	-0.06	-0.02		-0.19	0.06	-0.01	-0.04	0.02	0.00	-0.05	0.01	-0.02	-0.10	-0.15	-0.07	-0.03	
σ2	0.06	0.06		0.18	0.05	0.06	0.05	0.04	0.05	0.06	0.03	0.03	0.16	0.17	0.16	0.09	
mL	-0.04	-0.08	C2S4	0.00	0.10	-0.07	0.06	0.06	-0.04	-0.06	-0.02	-0.05	-0.07	-0.04	0.01	0.03	**C2S1***
σ1	0.14	0.20		0.09	0.11	0.32	0.06	0.03	0.24	0.14	0.11	0.18	0.13	0.07	0.05	0.08	
mQ	-0.01	-0.03		0.02	0.09	-0.01	0.05	0.05	0.01	-0.03	0.00	-0.01	-0.04	-0.03	0.01	0.02	
σ2	0.09	0.09		0.05	0.10	0.08	0.05	0.03	0.06	0.08	0.06	0.09	0.07	0.04	0.05	0.07	
mL	-0.05	-0.06	C2S5	0.14	0.15	0.02	0.08	0.14	0.03	0.04	0.09	0.09	**	0.07	0.08	0.17	C2S6
σ1	0.18	0.14		0.08	0.02	0.37	0.16	0.04	0.29	0.18	0.14	0.25	0.00	0.57	0.45	0.07	
mQ	-0.07	-0.05		0.14	0.14	0.06	0.09	0.14	0.06	0.07	0.11	0.13	**	0.13	0.13	0.17	
σ2	0.15	0.14		0.04	0.03	0.11	0.13	0.05	0.09	0.11	0.05	0.08	**	0.41	0.34	0.06	
mL	0.02	-0.05	C3S1	0.05	0.08	-0.12	-0.02	0.08	-0.08	-0.04	0.01	-0.04	0.01	0.00	-0.01	0.01	C3S5
σ1	0.11	0.17		0.03	0.06	0.27	0.09	0.04	0.18	0.12	0.12	0.14	0.13	0.07	0.05	0.07	
mQ	0.05	0.02		0.05	0.05	-0.02	-0.01	0.07	-0.01	-0.01	0.03	0.00	0.04	0.01	0.00	0.00	
σ2	0.07	0.08		0.03	0.05	0.08	0.08	0.04	0.05	0.06	0.04	0.05	0.05	0.03	0.05	0.06	
mL	-0.02	-0.07	C3S2	0.07	0.09	-0.07	-0.01	0.07	-0.03	-0.07	0.03	-0.05	-0.05	-0.04	-0.02	0.00	C3S2
σ1	0.16	0.23		0.05	0.08	0.27	0.09	0.04	0.19	0.12	0.07	0.16	0.15	0.09	0.08	0.08	
mQ	0.04	0.03		0.06	0.07	0.00	0.00	0.06	0.01	-0.04	0.04	0.00	-0.01	-0.01	-0.01	-0.02	
σ2	0.06	0.08		0.06	0.06	0.09	0.08	0.03	0.08	0.08	0.02	0.05	0.07	0.06	0.07	0.06	
mL	-0.05	-0.07	C3S3	0.00	0.03	-0.12	-0.06	0.00	-0.09	-0.10	-0.03	-0.11	-0.10	-0.12	-0.08	-0.04	C3S3
σ1	0.22	0.29		0.07	0.09	0.29	0.06	0.08	0.20	0.11	0.09	0.17	0.13	0.08	0.06	0.11	
mQ	0.03	0.03		0.00	0.02	-0.06	-0.05	-0.01	-0.05	-0.07	-0.01	-0.07	-0.06	-0.10	-0.06	-0.05	
σ2	0.09	0.09		0.07	0.07	0.04	0.05	0.07	0.03	0.06	0.06	0.05	0.05	0.05	0.05	0.10	
mL	0.00	-0.04	C3S4	-0.03	0.07	-0.11	-0.06	0.05	-0.08	-0.05	-0.01	-0.04	-0.05	-0.07	-0.05	0.01	**C3S1***
σ1	0.16	0.22		0.04	0.14	0.26	0.13	0.03	0.16	0.16	0.12	0.20	0.18	0.15	0.09	0.09	
mQ	0.04	0.01		-0.03	0.05	-0.06	-0.05	0.05	-0.05	-0.02	0.01	0.00	-0.01	-0.03	-0.04	0.00	
σ2	0.08	0.10		0.04	0.11	0.07	0.12	0.03	0.04	0.08	0.05	0.09	0.07	0.08	0.08	0.08	
mL	-0.15	-0.12	C3S5	0.09	0.08	-0.01	-0.04	0.03	0.00	-0.05	0.02	0.01	-0.08	-0.08	-0.08	-0.02	C3S6
σ1	0.22	0.19		0.05	0.07	0.28	0.05	0.07	0.23	0.11	0.08	0.16	0.19	0.16	0.09	0.10	
mQ	-0.16	-0.10		0.09	0.08	0.01	-0.04	0.02	0.02	-0.03	0.02	0.03	-0.06	-0.06	-0.07	-0.03	
σ2	0.21	0.19		0.05	0.05	0.08	0.05	0.05	0.06	0.07	0.05	0.06	0.08	0.08	0.07	0.08	

KEYS: mL= Mean of Calibration Accuracy
σ1= Standard Deviation of Calibration Accuracy
mQ= Mean of Residuals of Quadratic Fits
σ2= Standard Deviation of Residuals of Quadratic Fits

** Bad Data
* Data were waived

Table 8. Samples of AMSU-A1-1 instrument (RF Shelf) temperature variation* during one subcycle of scene temperature settings.

PRT Scene Temp. (K)	RF Shelf Temp. (C)
84.00	16.5
104.59	16.1
129.70	15.9
154.48	17.0
179.53	16.9
204.75	16.9
229.73	17.0
254.52	17.3
279.51	17.8
304.42	18.5
330.16	18.9

* Cycle 1, Sub2

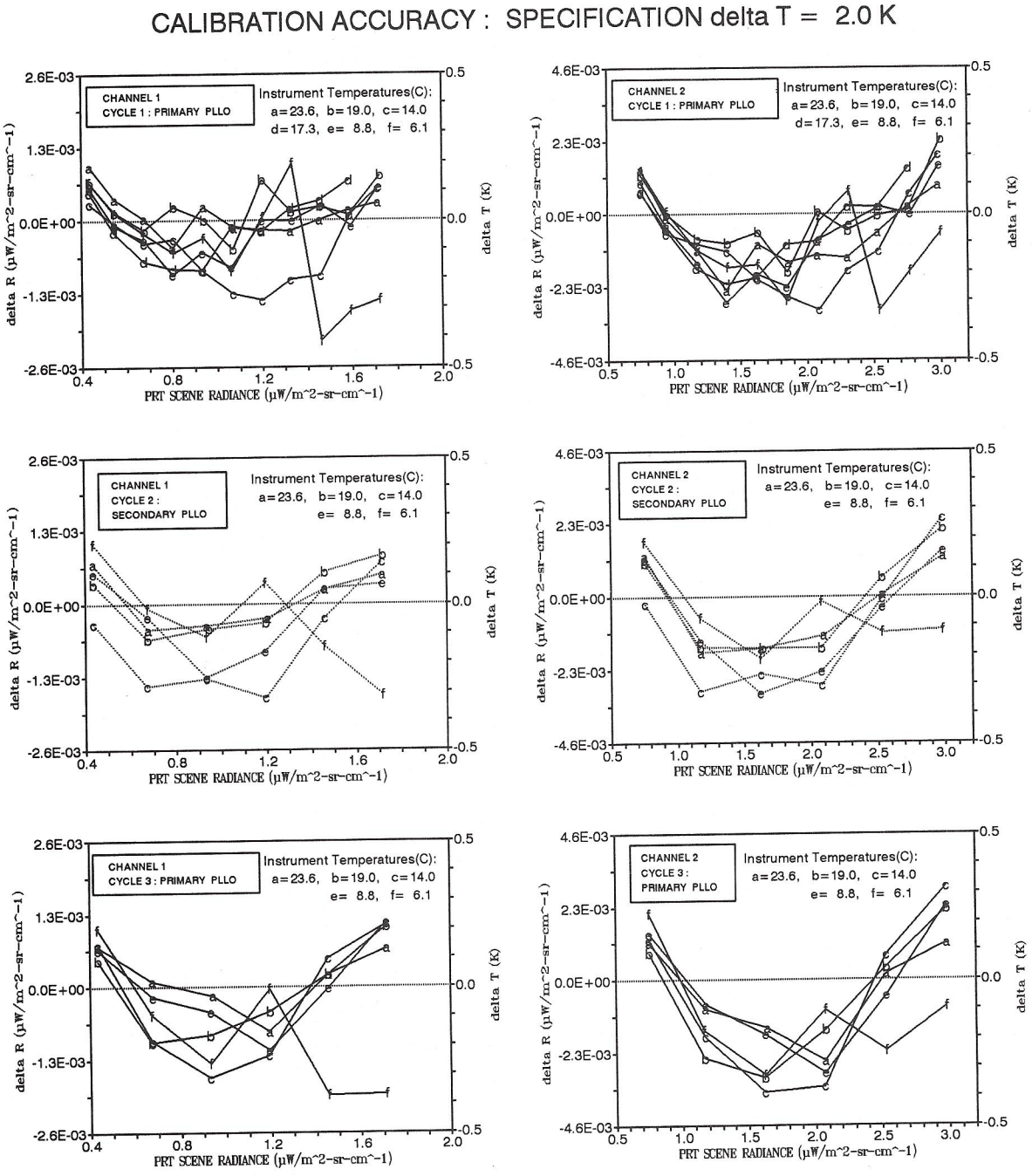

Figure 1. Calibration accuracies(ΔR) versus PRT scene-target radiances for Channels 1 and 2. The corresponding values in brightness temperature (ΔT) are given at the right-hand sides. Each curve corresponds to different instrument (RF Shelf) temperature as listed in each plot.

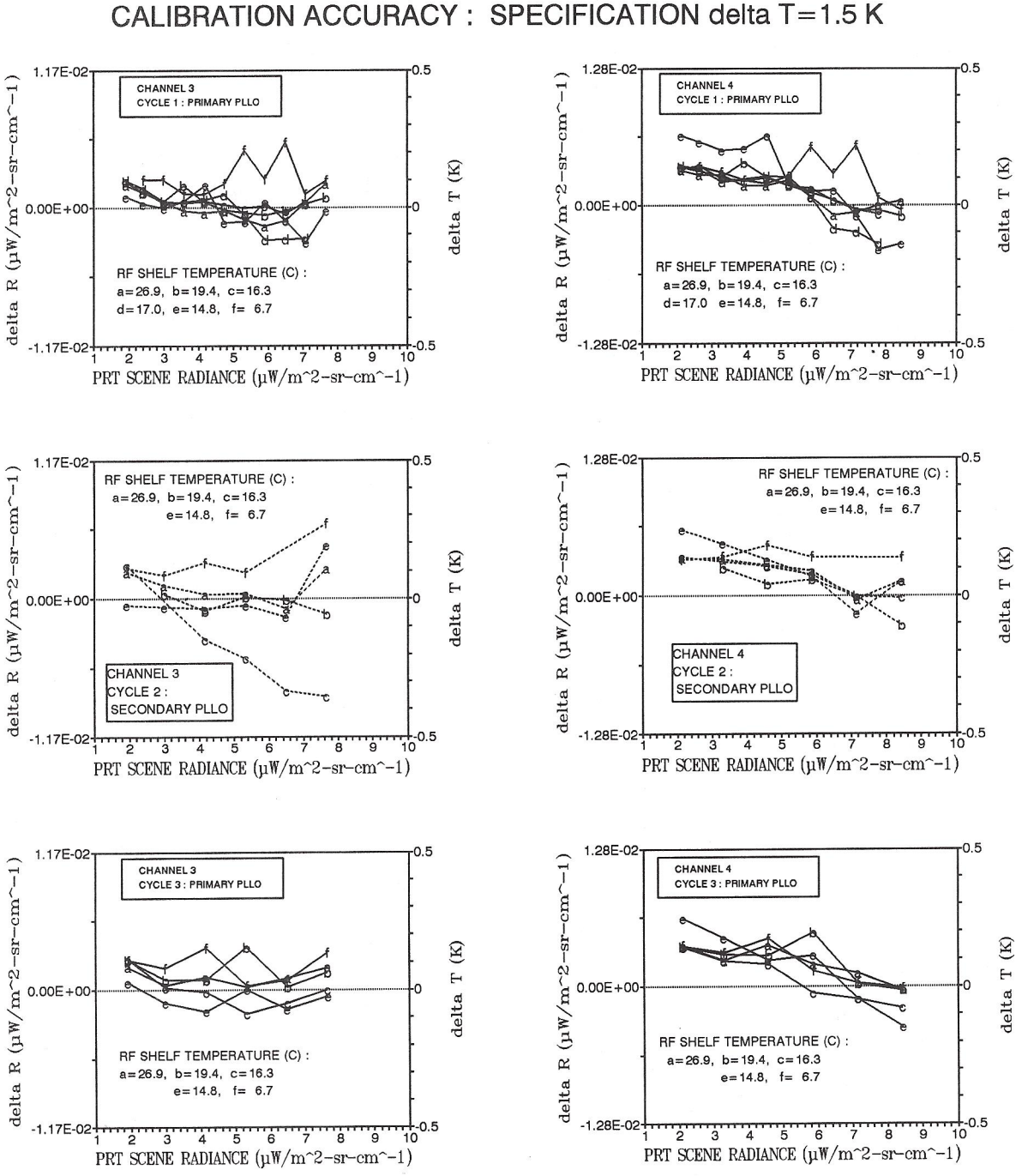

Figure 2. Calibration accuracies (ΔR) versus PRT scene-target radiances for Channels 3 and 4. The corresponding values in brightness temperature (ΔT) are given at the right-hand sides. Each curve corresponds to different instrument (RF Shelf) temperature as listed in each plot.

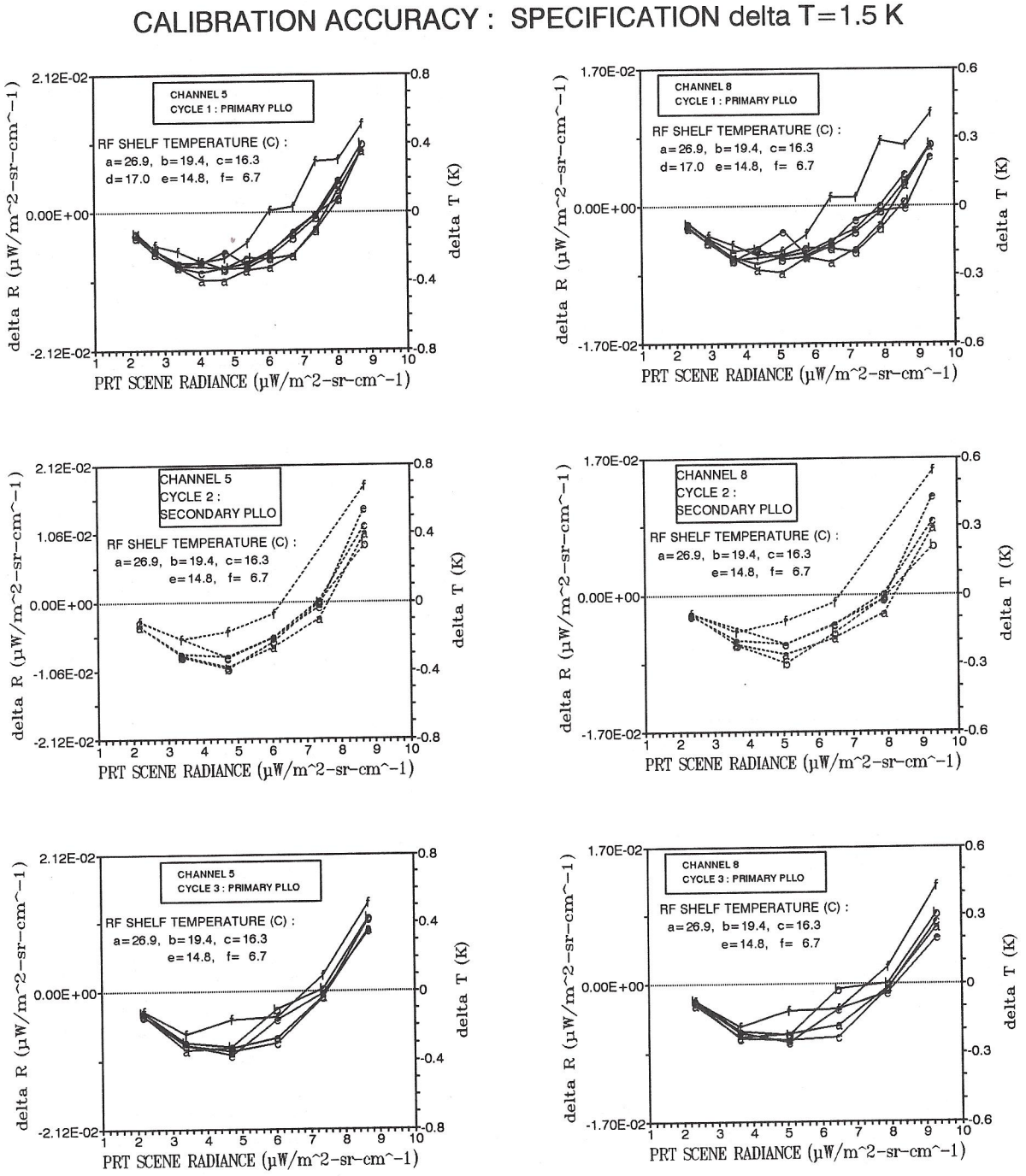

Figure 3. Calibration accuracies (ΔR) versus PRT scene-target radiances for Channels 5 and 8. The corresponding values in brightness temperature (ΔT) are given at the right-hand sides. Each curve corresponds to different instrument (RF Shelf) temperature as listed in each plot.

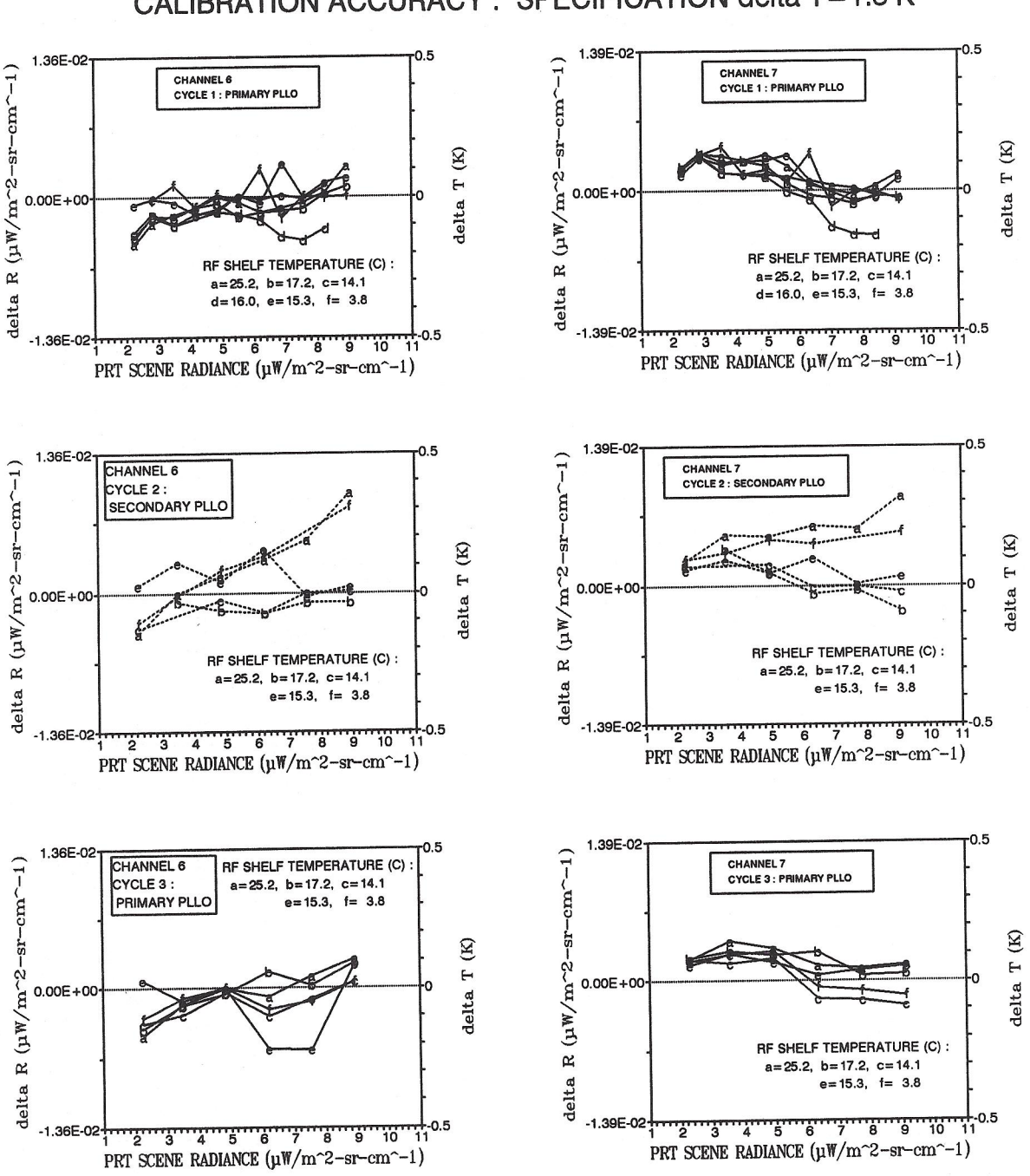

Figure 4. Calibration accuracies (ΔR) versus PRT scene-target radiances for Channels 6 and 7. The corresponding values in brightness temperature (ΔT) are given at the right-hand sides. Each curve corresponds to different instrument (RF Shelf) temperature as listed in each plot.

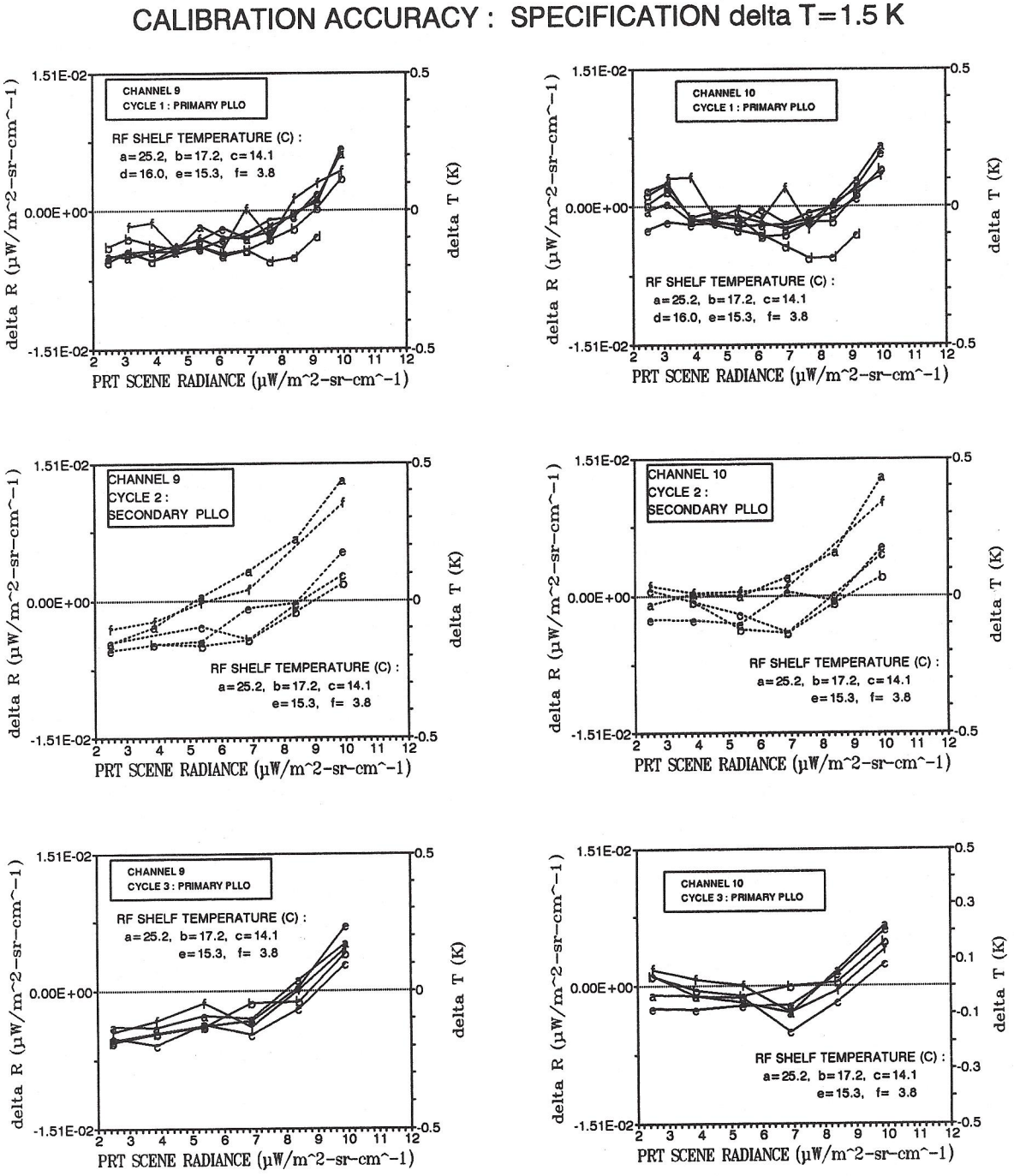

Figure 5. Calibration accuracies (ΔR) versus PRT scene-target radiances for Channels 9 and 10. The corresponding values in brightness temperature (ΔT) are given at the right-hand sides. Each curve corresponds to different instrument (RF Shelf) temperature as listed in each plot.

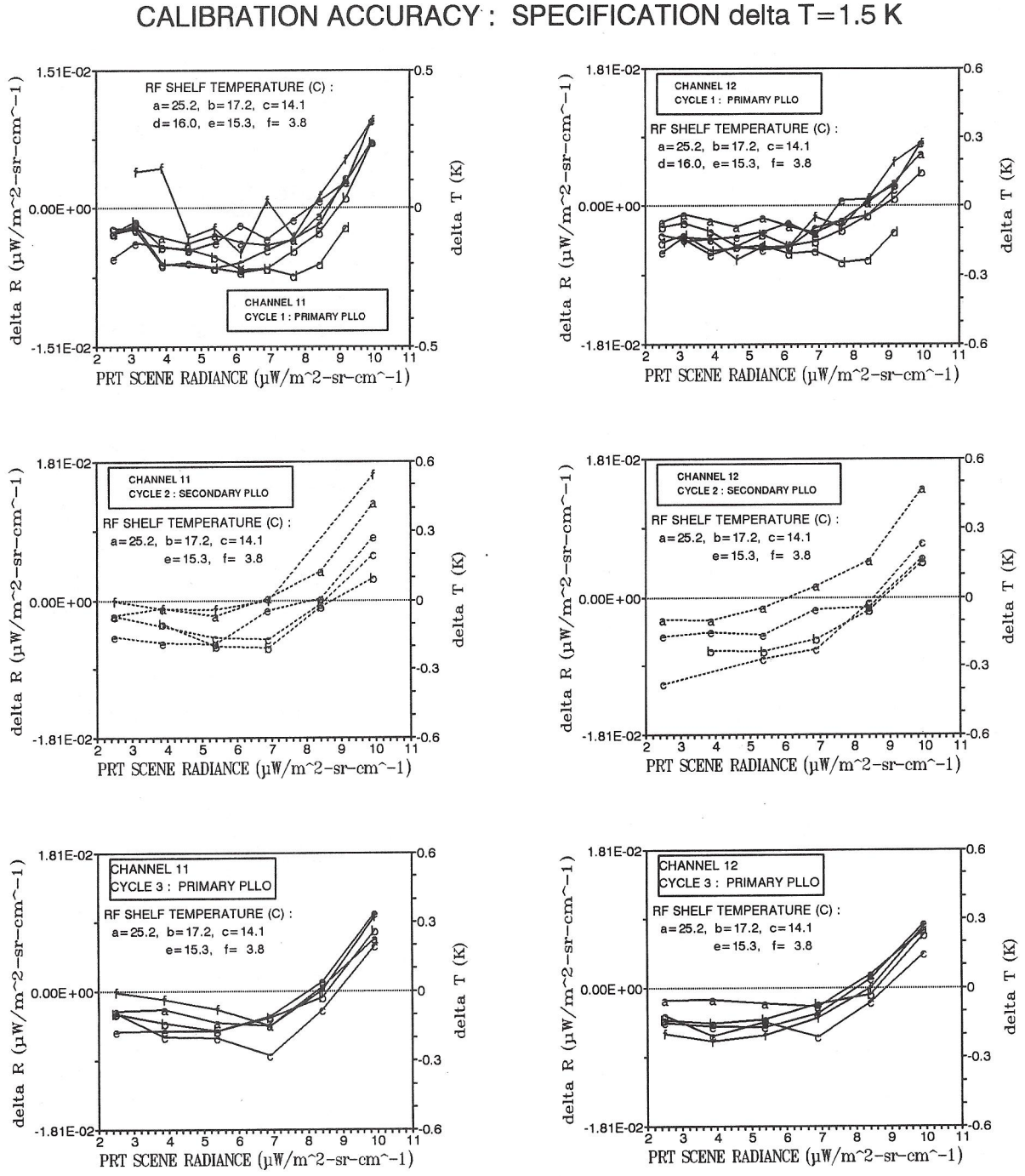

Figure 6. Calibration accuracies (ΔR) versus PRT scene-target radiances for Channels 11 and 12. The corresponding values in brightness temperature (ΔT) are given at the right-hand sides. Each curve corresponds to different instrument (RF Shelf) temperature as listed in each plot.

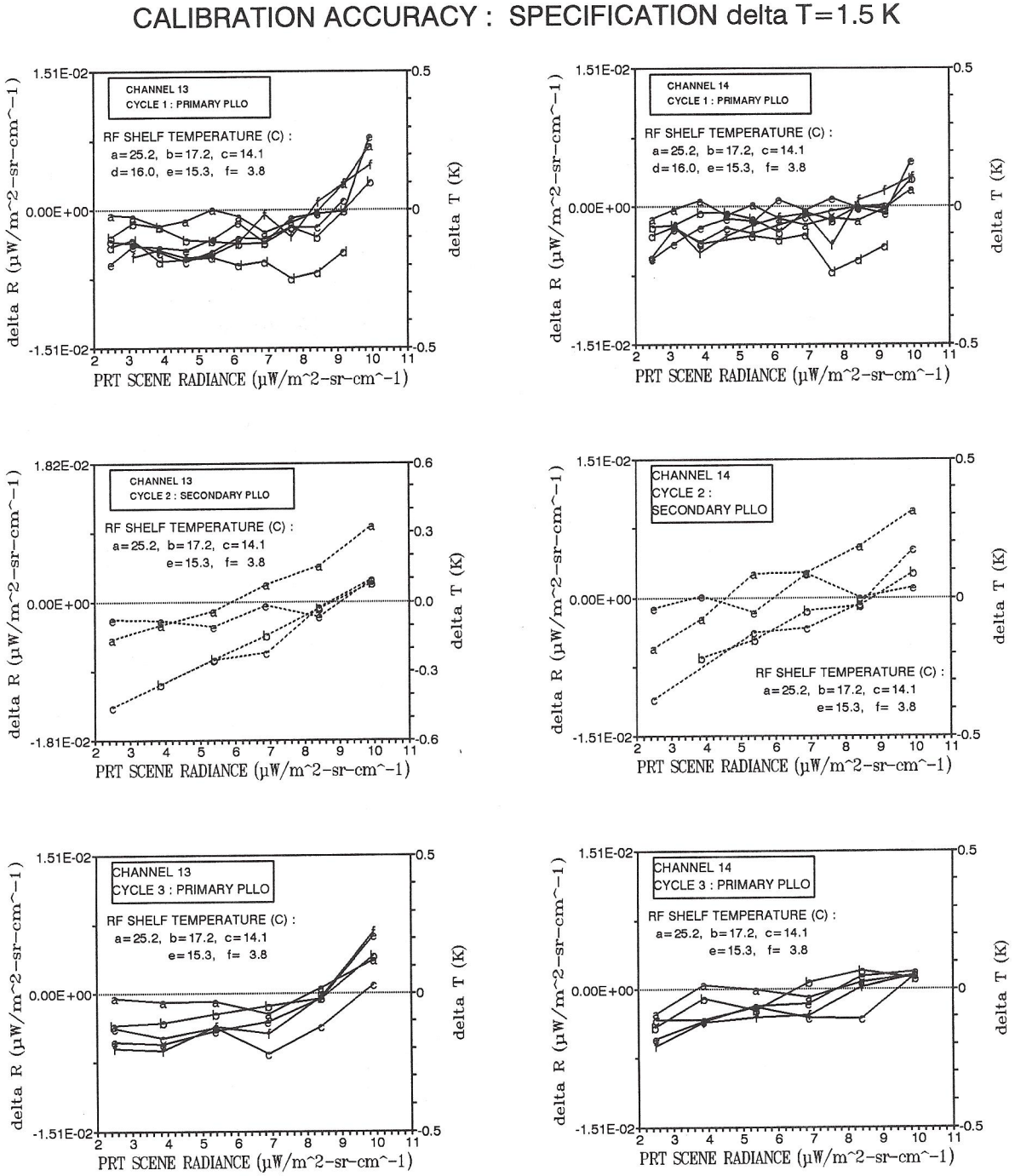

Figure 7. Calibration accuracies (ΔR) versus PRT scene-target radiances for Channels 13 and 14. The corresponding values in brightness temperature (ΔT) are given at the right-hand sides. Each curve corresponds to different instrument (RF Shelf) temperature as listed in each plot.

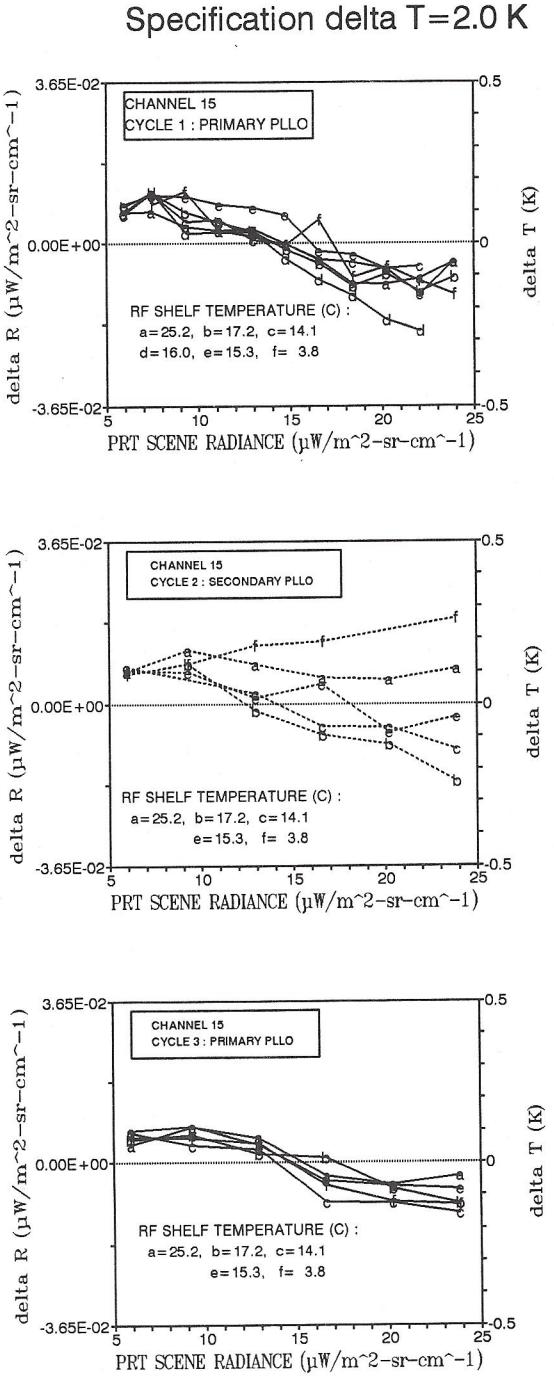

Figure 8. Calibration accuracies (ΔR) versus PRT scene-target radiances for Channel 15. The corresponding values in brightness temperature (ΔT) are given at the right-hand sides. Each curve corresponds to different instrument (RF Shelf) temperature as listed in each plot.

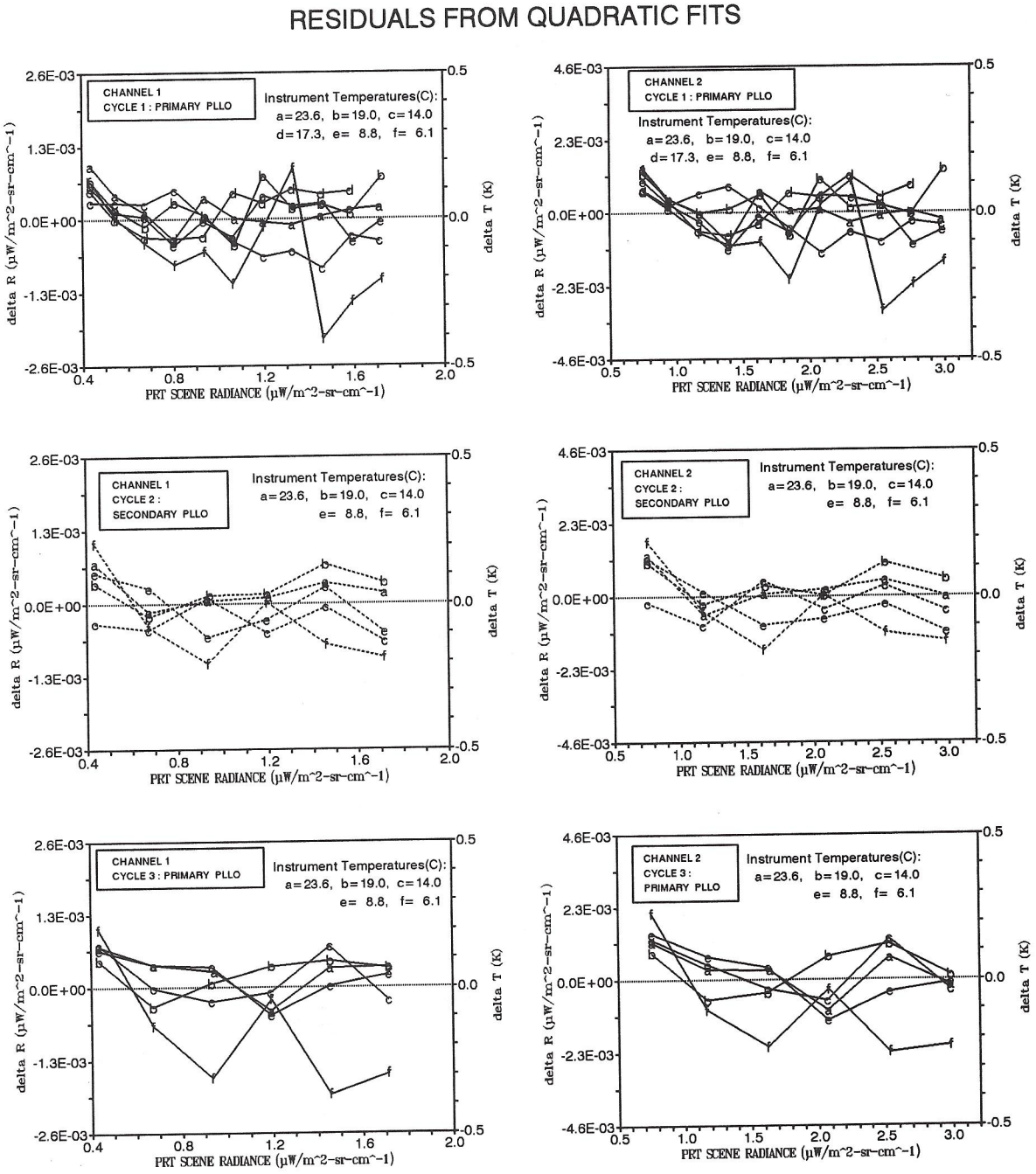

Figure 9. Residuals after applying the quadratic fits for channels 1 and 2.

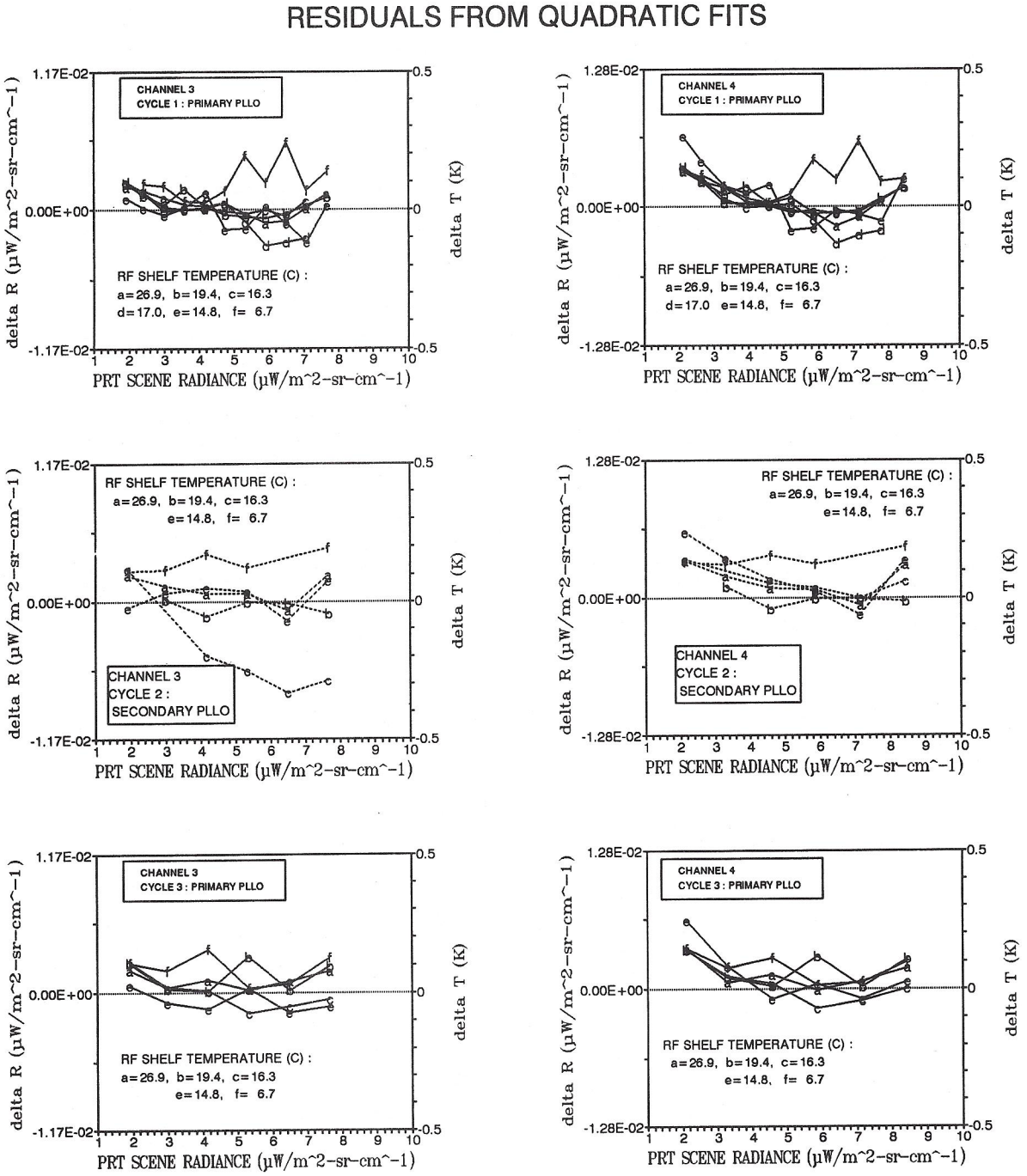

Figure 10. Residuals after applying the quadaratic fits for channels 3 and 4.

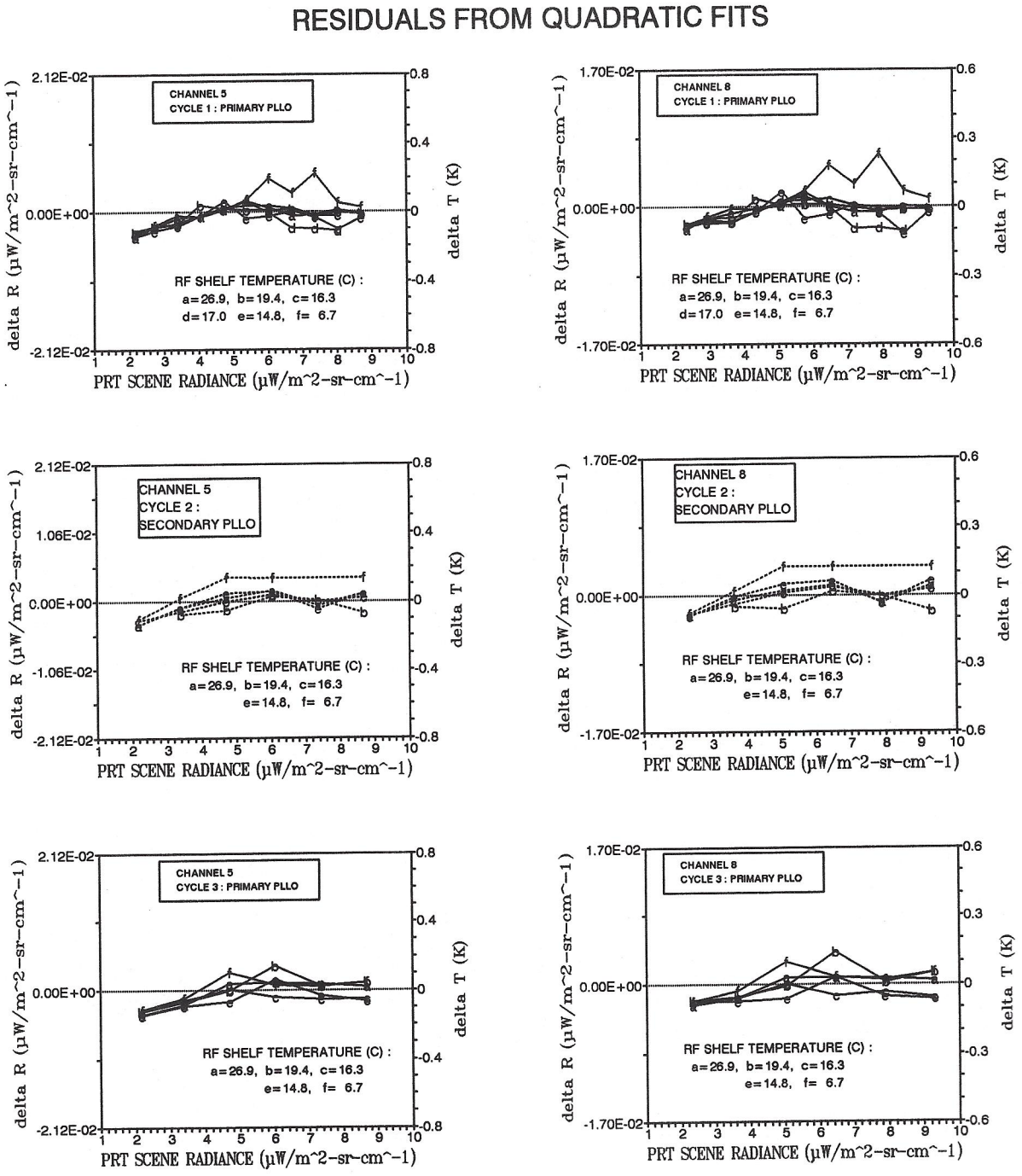

Figure 11. Residuals after applying the quadratic fits for channels 5 and 8.

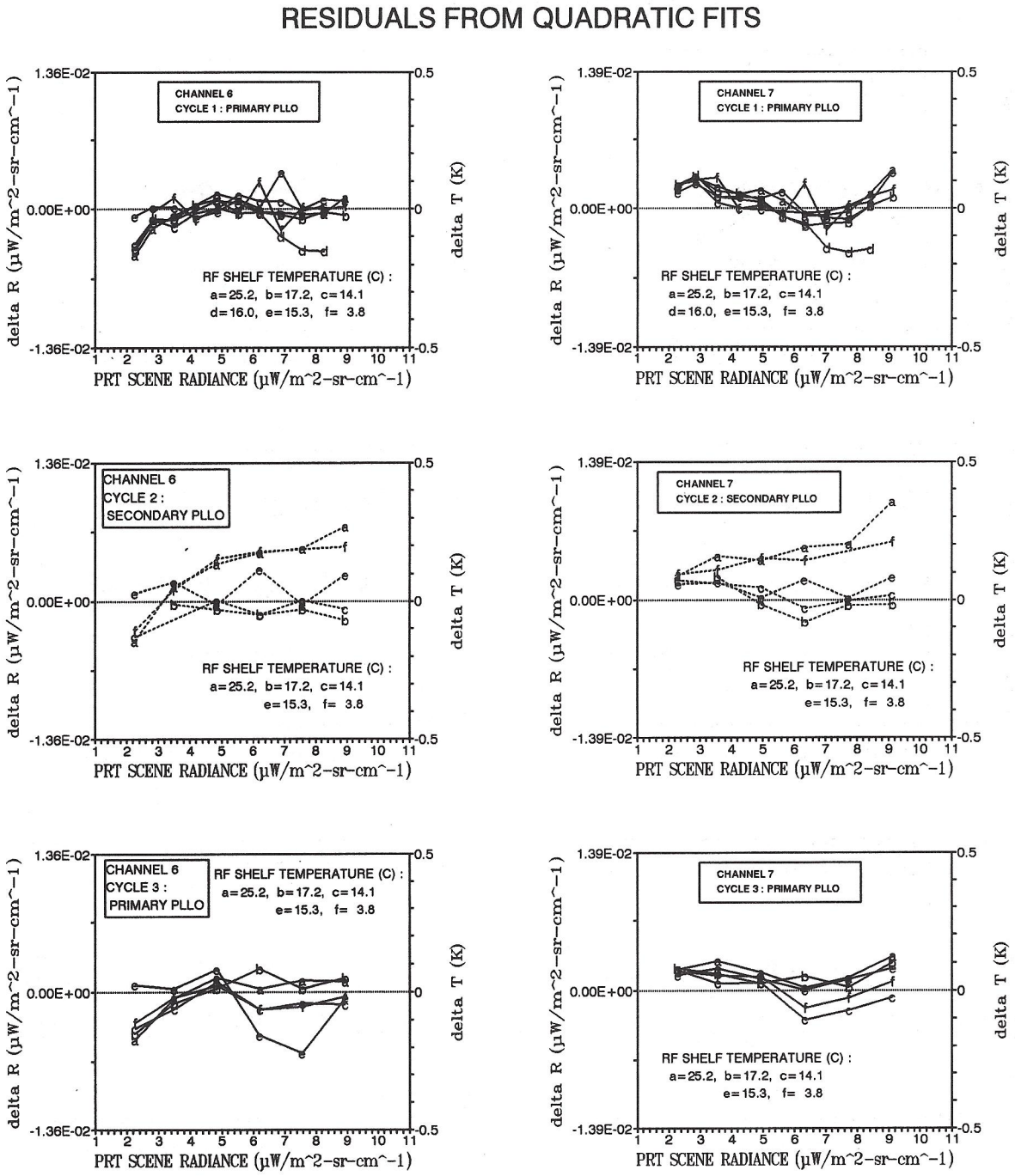

Figure 12. Residuals after applying the quadratic fits for channels 6 and 7.

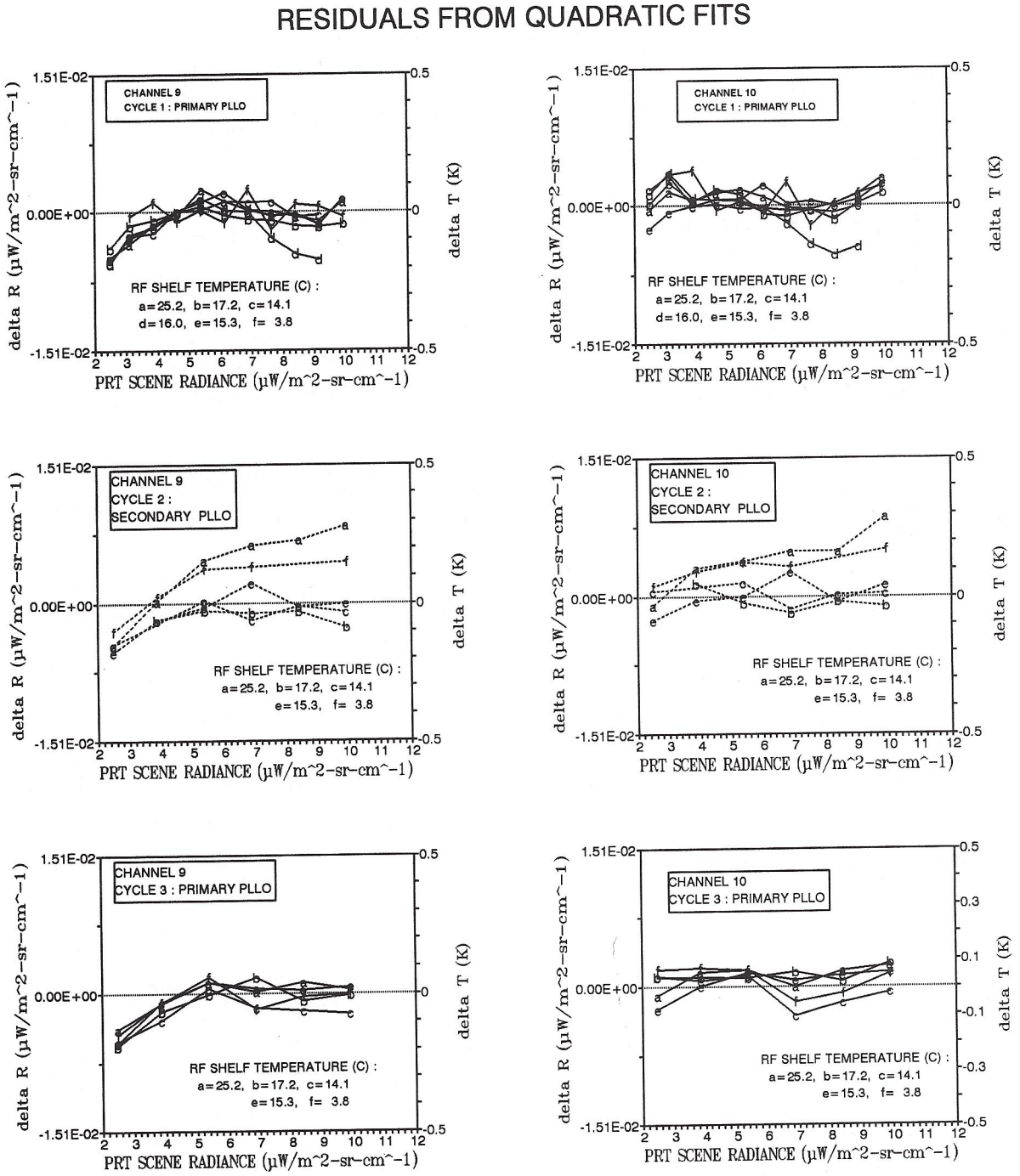

Figure 13. Residuals after applying the quadratic fits for channels 9 and 10.

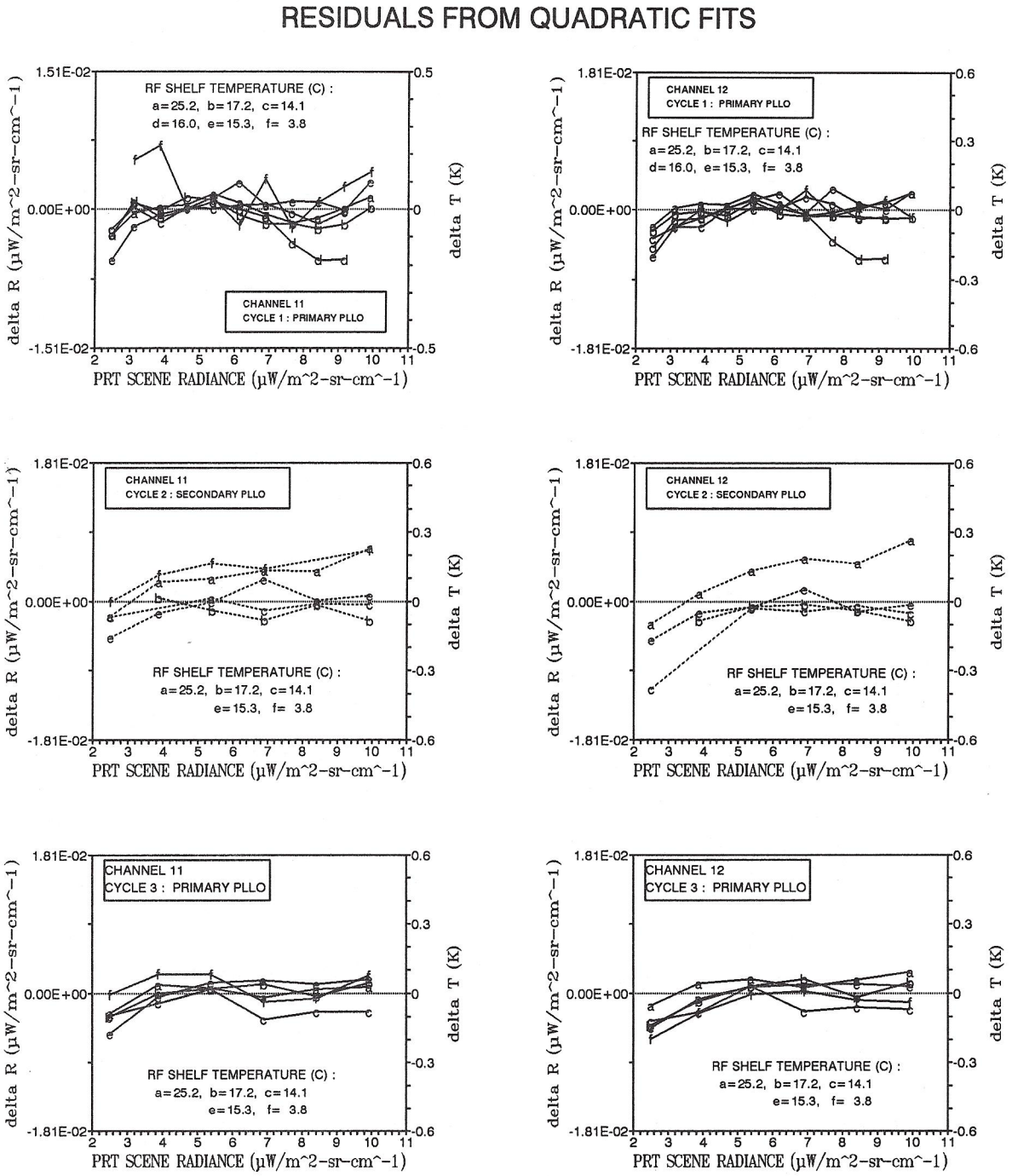

Figure 14. Residuals after applying the quadratic fits for channels 11 and 12.

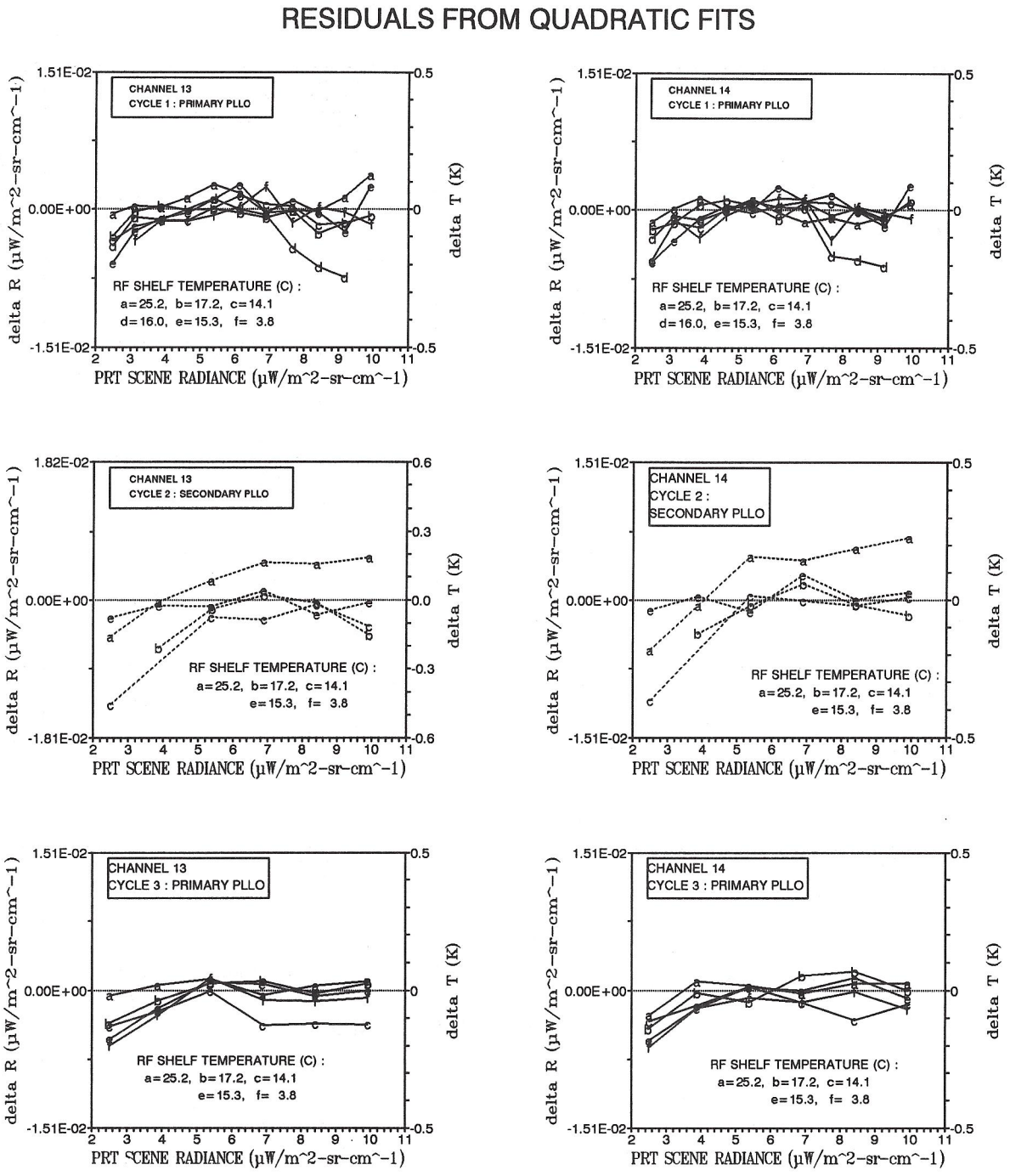

Figure 15. Residuals after applying the quadratic fits for channels 13 and 14.

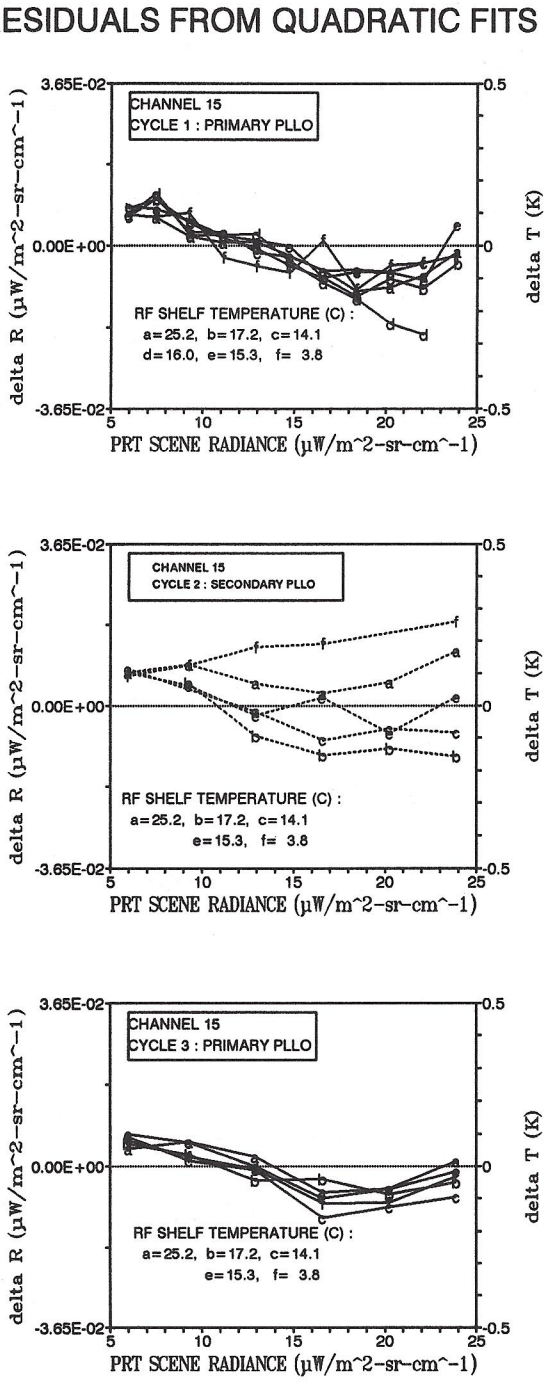

Figure 16. Residuals after applying the quadratic fits for channel 15.

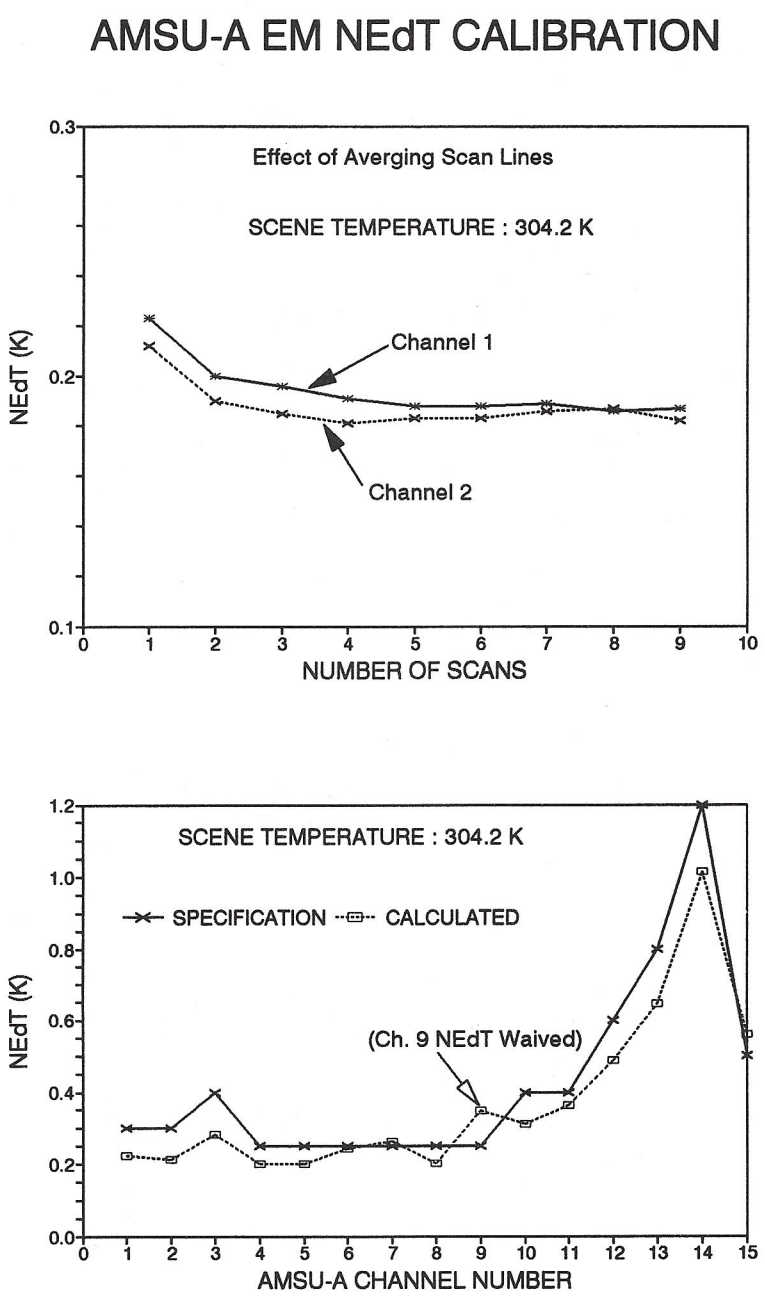

Figure 17. NEΔT Calibration. The lower part compares the calculated NEΔT values to the required values of instrument specifications at 15 channels. The upper part shows the effect of averaging the calibration parameters over number of scans on the NEΔT results.

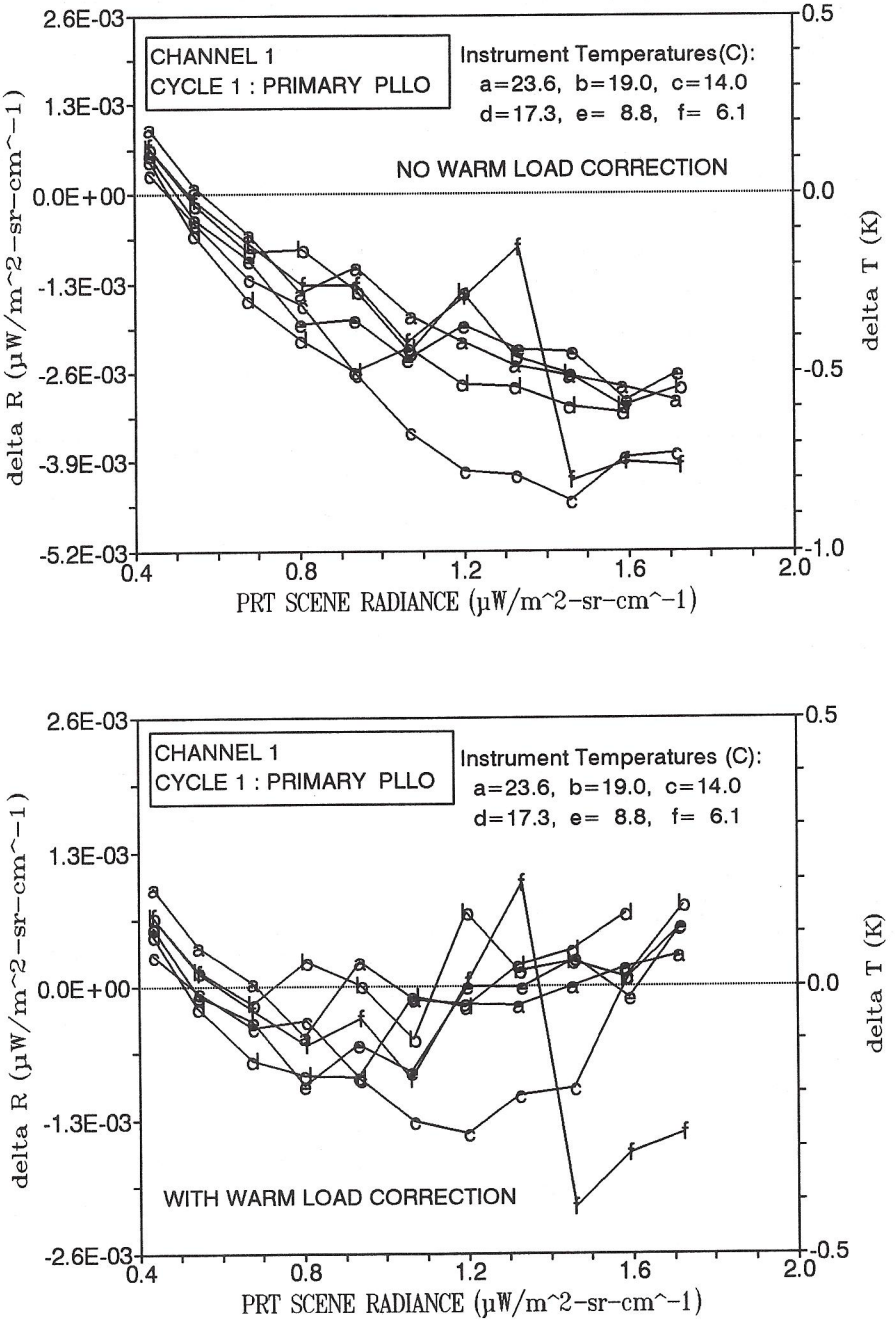

Figure 18. Effect of the warm target fixed bias correction factor R_{wo} on the calibration accuracy. Results in the top part were obtained with no warm load correction while those in the bottom part have warm load correction.

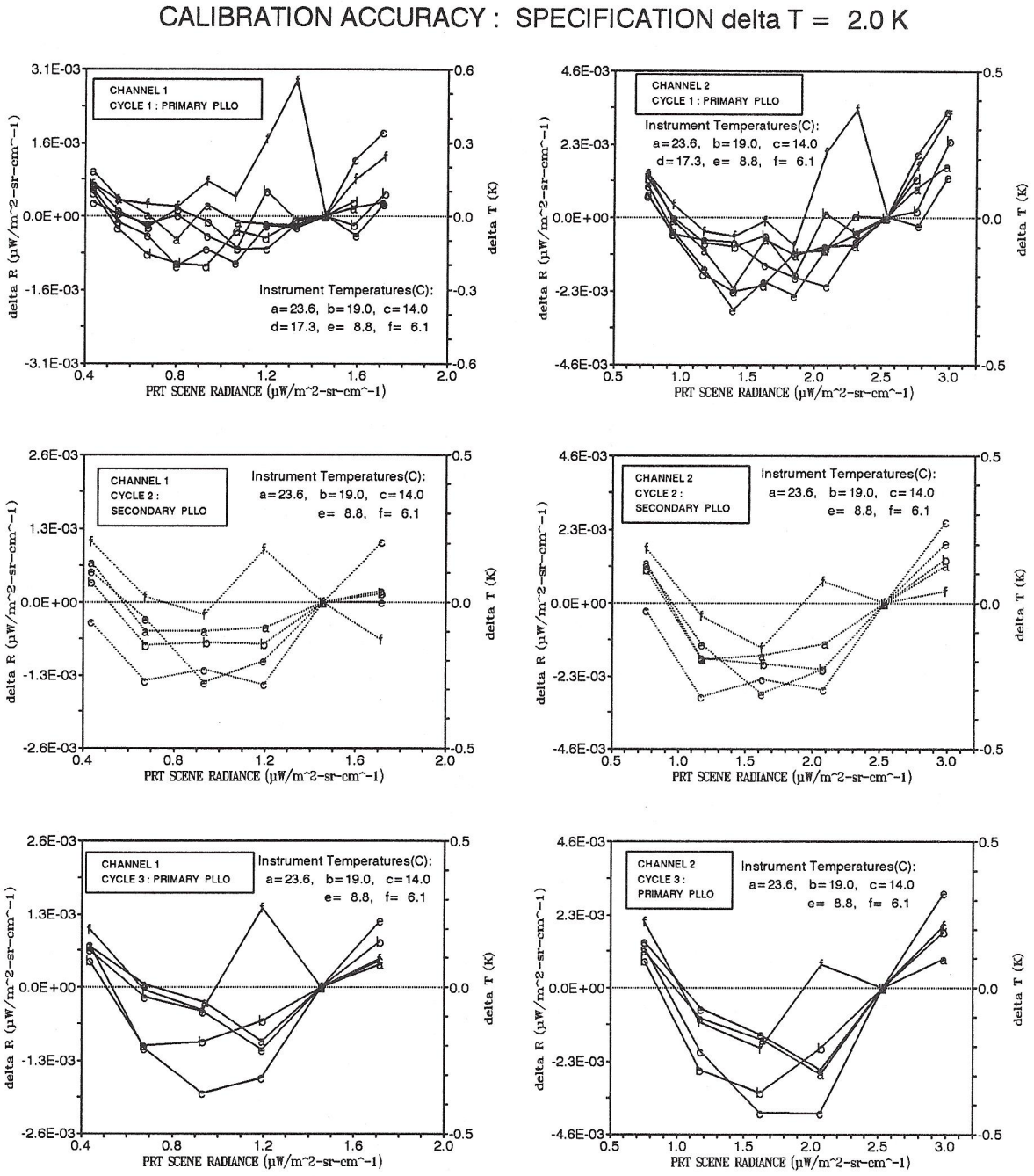

Figure 19. Calibration accuracies obtained with the R_{wo} values computed with the calibration data taken at the scene-target temperature T_s = 280K. One should compare these plots with those in Figure 1.

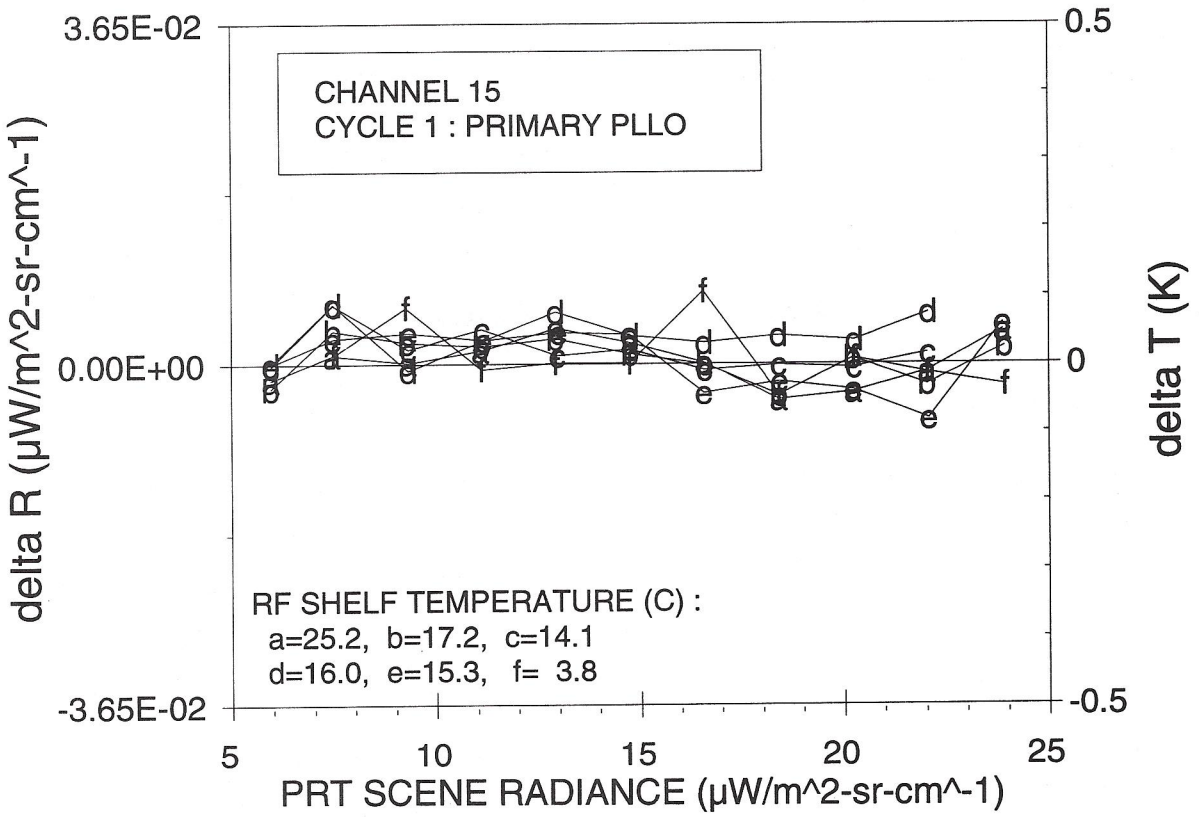

Figure B-1. Samples of least-squares fit results obtained with Equation (B-3). One should compare these plots with those in Figure 16.

*U.S. G.P.O.:1993-341-834:81062

NOAA SCIENTIFIC AND TECHNICAL PUBLICATIONS

The National Oceanic and Atmospheric Administration was established as part of the Department of Commerce on October 3, 1970. The mission responsibilities of NOAA are to assess the socioeconomic impact of natural and technological changes in the environment and to monitor and predict the state of the solid Earth, the oceans and their living resources, the atmosphere, and the space environment of the Earth.

The major components of NOAA regularly produce various types of scientific and technical information in the following kinds of publications:

PROFESSIONAL PAPERS - Important definitive research results, major techniques, and special investigations.

CONTRACT AND GRANT REPORTS - Reports prepared by contractors or grantees under NOAA sponsorship.

ATLAS - Presentation of analyzed data generally in the form of maps showing distribution of rainfall, chemical and physical conditions of oceans and atmosphere, distribution of fishes and marine mammals, ionospheric conditions, etc.

TECHNICAL SERVICE PUBLICATIONS - Reports containing data, observations, instructions, etc. A partial listing includes data serials; prediction and outlook periodicals; technical manuals, training papers, planning reports, and information serials; and miscellaneous technical publications.

TECHNICAL REPORTS - Journal quality with extensive details, mathematical developments, or data listings.

TECHNICAL MEMORANDUMS - Reports of preliminary, partial, or negative research or technology results, interim instructions, and the like.

U.S. DEPARTMENT OF COMMERCE
National Oceanic and Atmospheric Administration
National Environmental Satellite, Data, and Information Service
Washington, D.C. 20233